EXPERIMENTAL AND NUMERICAL INVESTIGATION OF TOOL-PART INTERACTIONS IN COMPOSITES MANUFACTURING

by

Övül Özgü Özsoy

B.S., Mechanical Engineering, Boğaziçi University, 2005

Submitted to the Institute for Graduate Studies in
Science and Engineering in partial fulfillment of
the requirements for the degree of
Master of Science

Graduate Program in in Mechanical Engineering
Boğaziçi University

2008

EXPERIMENTAL AND NUMERICAL INVESTIGATION OF TOOL-PART INTERACTIONS IN COMPOSITES MANUFACTURING

APPROVED BY:

Assist. Prof. Nuri B. Ersoy .....
(Thesis Supervisor)

Assoc. Prof. Fazıl Önder Sönmez .....

Assist. Prof. Melih Papila .....

DATE OF APPROVAL: 24.January.2008

ACKNOWLEDGEMENTS

Firstly I would like to express my gratitude to my advisor Assist. Prof. Nuri Ersoy for offering me his full support and encouragement throughout the course of this research, for his patience and time throughout my study.

I would also like to acknowledge the help of Prof. Dr. Michael Wisnom and Dr. Kevin Potter, who patiently guided me throughout my work, constantly watched over my progress and repeatedly answered my questions on technical issues during my visit at the University of Bristol. I would like to thank to Bogazici University Research Fund (Project Code: 07A606), and University of Bristol for the sponsorship for this research.

It would not have been possible to conduct my work in University of Bristol without the help of Simon Johns and Carwyn Ward in all things to do in the laboratory. Thank you very much for your patience and support and, especially, friendship.

I would also like to thank Erhan Turan and Utku Ünlü for their help in all things to do with analytical work, their patience and support. I am also thankful to my research assistant colleagues in the Mechanical Engineering department, Boğaziçi University for their support and friendship during my study.

The assistance and support and friendship of all members of the ACCIS(Advanced Composites Centre for Innovation and Science) and Aerospace Engineering department, University of Bristol, were greatly appreciated.

There are no words that could express my gratitude for the love and encouragement provided by my family during my entire education. Without them, this thesis would not have been written.

ABSTRACT

EXPERIMENTAL AND NUMERICAL INVESTIGATION OF TOOL-PART INTERACTIONS IN COMPOSITES MANUFACTURING

Composite parts may undergo some shape distortions due to the residual stresses generated during the cure cycle. This may cause difficulties in assembling composite structures. This experimental and numerical work is done to investigate shape distortions, and stress distributions built up during manufacturing due to tool-part interaction.

In the numerical study, tool-part interaction induced warpage effects are modeled for flat composite strips in three different ways by using a three step finite element analysis procedure. The analysis is based on a number of simplifying assumptions, most of which are reasonable. Vitrification is treated as a point at which the material suddenly changes from the rubbery to glassy state with constant properties in each case.

The models developed take into account the observations on the interactions between the tool and the part and between the prepreg layers themselves, and a work has been carried out to investigate the effect of various process parameters and interface properties on the manufacturing distortions of composite parts.

Elasticity solutions were made to compare the results of the two finite element models mentioned above. A closed-form analytical model based on the theory of elasticity is implemented to analyze the process- induced stresses and deformations that develop during the cure cycle of a composite flat part. Solutions were obtained for the sticking and sliding boundary conditions.

Through tension test, by loading and unloading a single uncured ply, a load displacement data obtained, which is then converted into stress-strain relation. The difference between the loading and unloading curves reveals the initial waviness of fibers. The effect of this behavior on fibre stress development due to tool-part interaction is analyzed.

Tool-part investigation is further investigated by marked-tool test. This test is a new method to measure the degree of tool-part interaction.

End observations were made through image analysis of the samples cut from the corners of both ends of the specimens under the optical microscope.

These experimental observations are tried to be explained by the help of analytical tools developed.

ÖZET

KOMPOZİT İMALATINDA KALIP-PARÇA ETKİLEŞİMLERİNİN DENEYSEL VE SAYISAL ARAŞTIRMASI

Kompozit parçalar pişirme çevrimi sırasında oluşan artık gerilmelerden dolayı şekil bozukluklarına maruz kalırlar. Bu durum kompozit yapıların bir araya getirilmesinde zorluklara neden olmaktadır. Bu deneysel ve sayısal çalışma, düz kompozit parçalar için pişirme çevriminin basamakları sırasında meydana gelen şekil bozuklukları ve gerilme dağılımlarını incelemek üzere yapılmıştır.

Sayısal çalışmada,düz kompozit parçalarda kalıp-parça etkileşiminden kaynaklanan şekil çarpılmaları üç basamaklı bir sonlu elemanlar analizi kullanılarak üç değişik biçimde modellenmiştir. Analiz sırasında belirli sebeplere dayanan bazı basitleştirici varsayımlarda bulunulmuştur. Camlaşma, malzemenin birdenbire kauçuk durumdan camsı duruma geçtiği bir nokta olarak düşünülmüştür. Her iki durumda da sabit malzeme özellikleri bulunmaktadır.

Geliştirilen modellerde kalıp ve parça etkileşiminin yanısıra katmanlar arasındaki etkileşim de dikkate alınmıştır. Çalışma, çeşitli işlem parametrelerinin ve arayüzey özelliklerinin, kompozit parçaların üretim çarpılmalarına etkisi araştırılmıştır.

Yukarıda sözü edilen iki sonlu elemanlar yönteminin sonuçlarını karşılaştırmak için elastisite çözümleri yapılmıştır. Kompozit bir parçanın pişirme çevrimi sırasında oluşan gerilme ve şekil bozukluklarını çözümlemek için elastisite teoremine dayalı kapali formda sayısal bir model uygulanmıştır. Tutunma ve kayma sınır koşulları için çözümler elde edilmiştir.

Çekme deneyinde, pişmemiş tek bir kat yuklenip boşaltılarak, yük-yer değiştirme verisi elde edilmiş ve bu veri daha sonra gerilme-gerinme ilişkisine çevrilmiştir. Yükleme ve boşaltma eğrileri arasındaki fark liflerin başlangıçta düz değil dalgalı olduğunu ortaya koymaktadır. Bu durumun kalıp-parça etkileşiminden dolayı, lifler üzerinde gerilme oluşumuna etkisi de incelenmiştir.

Kalıp-parça etkileşimi ayrıca işaretli kalıp testi ile de incelenmiştir. Bu test kalıp-parça etkileşiminin derecesini ölçmek için yeni bir yöntemdir.

Uç gözlemleri, numunelerin iki ucunun köşelerinden kesilen kompozit örneklerini optik mikroskopta inceleyerek yapılmıştır.

Bu deneysel çalışmalar geliştirilen sayısal yöntemlerle açılanmaya çalışılmıştır.

TABLE OF CONTENTS

LIST OF FIGURES

LIST OF TABLES

LIST OF SYMBOLS/ABBREVIATIONS

E	Young's modulus
G	Shear modulus
p	Pressure
T	Temperature
t	Thickness
u	Displacement
α	Coefficient of thermal expension
δ	Difference between two values
Δ	Difference between two values
ε	Strain
ν	Poisson's ratio
σ	Normal stress
τ	Shear stress
$\tau_{t/p}$	Maximum shear stress between the tool and the part
$\tau_{p/p}$	Maximum shear stress between the ply adjacent to the tool and the rest of the plies

BC	Boundary condition
CTE	Coefficient of thermal expansion
FE	Finite element
FEA	Finite element analysis
FEM	Finite element method
MRCC	Manufacturer's recommended cure cycle
UD	Uni-directional

1. INTRODUCTION

Composite parts may have some shape distortions due to the residual stresses developing during the cure cycle, interaction with the tool and applied vacuum pressure. This can cause difficulties in assembling composite structures. This experimental and numerical work is done for calculating the distortions which are generated during the cure cycle for different lay-ups of flat composite strips.

Moreover, both chemically induced shrinkage and thermal deformations are generated during composite processing. The fibers possess a very small thermal expansion coefficient along their longitudinal axis and that produces little deformation in that direction during resin cure. The polymer matrix has a much higher thermal expansion coefficient and is thus more susceptible to temperature changes. The difference of the thermal expansion coefficients in the fibre and transverse directions is one of the major sources of the residual stresses. After the cure of fiber-reinforced composites, the residual stresses generated can have considerable effects on the part quality and on its mechanical properties, promoting warpage or initiating matrix cracks and delamination [1].

Sources of manufacturing distortions in composite manufacturing and their relative contributions to the final shape of the composite parts have attracted recently considerable research effort. One of the sources of manufacturing distortions that have attracted considerable reserach effort is tool-part interaction. The resulting distorted shapes consistently show a convex up curvature as the middle of the flat symmetric part lifts away from the tool. A number of parameters were found to affect the measured warpage in flat sections, the most prominent being the mismatch of coefficient of thermal expansions (CTE) between the tooling and the component [2]. Other factors are through-the-thickness fibre volume fraction gradients, lay-up orientation, part thickness and shape, use of release agent/film and the cure cycle [3, 4].

When the laminate is laid on a tool that has a considerably higher CTE and the consolidation pressure is applied, a shear interaction develops at the tool-part interface during the temperature ramps of the Manufacturer's Recommended Cure Cycle (MRCC), putting the tows close to the tool surface in tension. This occurs at the early stages of the cure, before the resin cures, when the resin modulus is low, causing a decay of tensile stresses away from the tool surface. This stress profile is locked in as the cure completes and when the part is removed from the tool, the locked in stresses cause a bending moment, forcing the part to warp in a concave-up sense (Fig. 1.1).

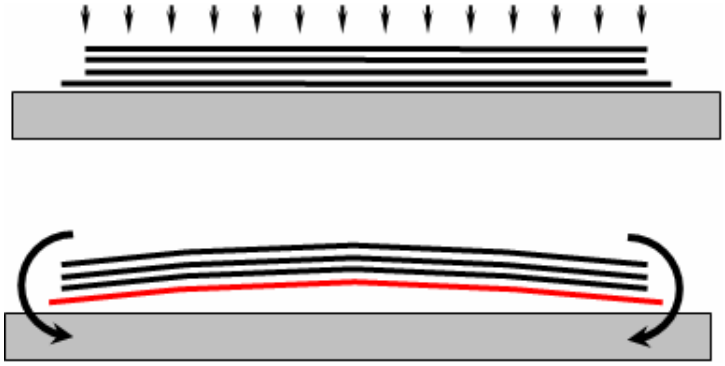

Figure 1.1. Warping of flat laminates due to tool interaction[18]

Other researchers emphasized the effect of tool-part interaction on spring-in [5, 6, 7, 8], all agreeing that the tool interaction causes an increase in measured spring-in angle of corner sections manufactured on male tools and a decrease in female tools. It is not clear if the tool-part interaction has an effect on the spring-in of the curved section, or if the measured difference is due to arm bowing in the flat sections.

Another shear process occurring during manufacturing of composite parts is the slippage of the prepreg layers with respect to each other. This mechanism, which has to date received little research attention, is effective in manufacturing rather complex parts with corner sections. As the preform for the corner section is imperfect as laid-up, consolidation of the corner under autoclave pressure involves slippage of the prepregs with respect to each other, causing tensile stresses in the tows close to the inner radius, if the prepregs do not slip fully. These stresses are locked in as the part cures, contributing to the increase of the spring-in angle.

Since tool correction by trial and error is an expensive and time consuming task, the development of an analytical tool to predict the spring-in taking into account various factors has also attracted a considerable research effort, and tool-part interaction is also included in most process models as a major contributor to the final shape of the parts[8, 9, 10, 11]. In these models, tool-part interaction is either modeled as the part stuck to the tool surface with no relative motion [9], or as a cure hardening elastic shear layer which remains intact until the tool is removed [8, 10, 11]. By adjusting the properties of this shear layer, the amount of stress transferred between the tool and the part can be tailored. With the use of experimental data the shear layer properties were calibrated to an appropriate value. These simulations are based on semi-empirical models, which need to be calibrated according to geometrical deformations observed in manufactured parts.

Some recent studies concentrate on measuring the tool-part interaction using an instrumented tool. In [12] the researchers have developed a quantitative means of examining the interactions between the tool and the part by applying a strain gauge rosette on a thin aluminium tool and curing a composite part on that instrumented tool under vacuum. They found that during the heat-up portion of the cure cycle when residual stress development due to tool-part interaction is most significant, a sliding friction condition is prevalent at the tool-part interface. Furthermore, the degree of elastic constraint observed at low degrees of cure indicates an interaction between the fibre bed and the tool. This shows that even prior to resin gelation, the part can develop fibre stresses. However, the sensitivity of this study is limited due to the high stiffness of the tool, and the strains due to tool interaction are only a small fraction of the total measured signal. This methodology was later used to predict the warpage of flat laminates [13, 14].

A more direct approach was adopted by Kim and Daniel [15] by measuring the strains in the composite laminates during curing using embedded fibre optic strain sensors and electrical resistance strain gauges. It was found that significant strain was developed by interference between the composite and mould during cure, resulting in constraint-induced strain. However the strain gages and fibre optic sensors can pick up

strain readings only after gelation where the resin cures to the point that it can sustain stress. Recently Potter et al. [16] used a spot curing technique, where the strain gauges are bonded to cured spots on the prepreg, calibrated in a tensile test machine for load vs. strain. The prepreg is then cured under the MRCC, and the strains recorded. The data showed that the magnitude of the in-plane tensile stress is proportional to the distance from the free ends of the prepreg, indicating a sliding friction condition with constant shear stress at the tool-part interface.

Flanagan [17] measured the friction coefficients between the Fiberite Epoxy 934 prepreg and the tool surfaces treated by Frekote release agent with or without release film as a function of temperature and pressure. He used a heated plate, and dead weights to simulate the cure cycle, however, the maximum pressures he attained by this method is only a fraction of the autoclave pressure (0.24 versus 0.586 MPa). The friction coefficients are observed to be relatively independent of the pressure, and to decrease substantially as the resin is heated with a ramp of 2° C/min (1.14 at room temperature, 0.17 at 125° C), as the resin viscosity goes down. At about 160° C, which corresponds to the gel point, the friction coefficient increases to the value for the cured laminate (0.33). However, the values measured are the coefficients at the onset of slip, and the test method does not allow to measure very low post-slip friction coefficients. Also the tests do not represent the continuous relative slipping of the interfaces during the heat-up ramps of MRCC.

The tool-part interaction stresses were measured previously by Ersoy [18]. It has been found that the shear stresses between the prepreg/prepreg interfaces are higher than the shear stresses between the tool-prepreg interfaces for AS4/8552 composite. Fibre intermingling at the prepreg/prepreg interfaces is believed to cause higher shear stresses as compared to the fibre friction at the tool/part interfaces.

Wisnom et al. [19] investigated the mechanisms generating stresses and distortions during the cure. They suggested that distortions generated primarily due to thermal stresses during cooldown arising after vitrification. At that point, the material has developed significant stiffness. It develops progressively as the T_g increases

with cure. They concluded that spring-in is effected also by thermal stresses and cure shrinkage in the rubbery state, due to tool-part interaction and significant fibre stresses may develop during the initial stages of cure where the resin is in viscous state.

Arafath [20] presented a closed- form solution based on the theory of elasticity to analyze the process-induced stresses and deformations that develop during the cure cycle of a composite flat part. These solutions showed that the in-plane stress gradient in the thickness direction depends on both material and the geometry of the part.

All the previous experimental data show that there is a sliding friction condition at the tool-part interface during the heat up ramps in a MRCC. However, none of the previous work offers an extensive understanding of the shear processes at the tool-part as well as the prepreg-prepreg interfaces.

This study provides two new approaches. Firstly, FEA with a sliding friction condition between tool/part and prepreg/prepreg interfaces is investigated. Secondly, tool/part interaction is observed directly by marked-tool test and image analysis of the ends of the part.

The models developed take into account the observations on the interactions between the tool and the part and between the prepreg layers themselves, and a work has been carried out to investigate the effect of various process parameters and interface properties on the manufacturing distortions of composite parts.

Elasticity solutions were made to compare the results of the two finite element models mentioned above. A closed-form analytical model based on the theory of elasticity is implemented to analyze the process- induced stresses and deformations that develop during the cure cycle of a composite flat part. Solutions were obtained for the sticking and sliding boundary conditions.

2. EXPERIMENTAL WORK

2.1. Material Used

The prepreg investigated in this study is a unidirectional carbon/epoxy, produced by Hexcel Composites with a designation of AS4/8552. The nominal thickness of the prepreg was given as 0.125 mm. All the specimens were fabricated by lay-up of 1m long and 50 mm wide plies with a thickness ranging from 0.75 mm to 1.5 mm, which were cut by an automated cutting machine.

2.2. Manufacturing Process

All the manufacturing process was carried out at University of Bristol. Before using the autoclave, the tool was prepared. It is cleaned with acetone and Freekote release agent was applied for a good slip between the tool and the part. Two different tools were used during the experiments. Both of the them were made of aluminium with a good surface finish. The difference between them was that the tool used for the marked-tool test was scratched at every 100 mm.

Flat composite parts were prepared with various lay-ups. They were carefully placed on the tool directly, then they were covered with a release film and a breather cloth, and vacuum bagged.

Finally, they were cured in the autoclave with a 0.7 pressure applied on it using the Manufacturer's Recommended Cure Cycle, MRCC, shown in Fig.2.1. The MRCC consists of a first ramp of 2° C/min up to 120° C and a first hold at 120° C for 60 min, a second ramp of 2° C/min up to 180° C and a second hold at 180° C for 120 min. A pressure of 0.7 MPa is applied throughout the cycle.

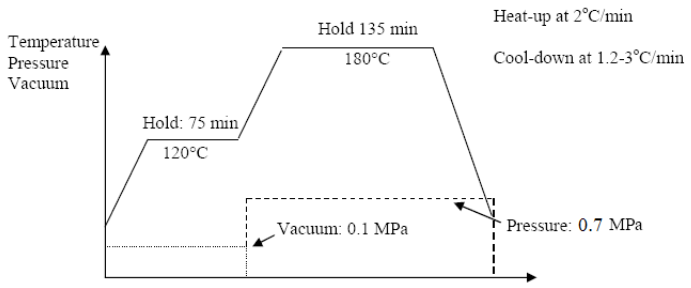

Figure 2.1. Manufacturer's recommended cure cycle

2.3. Marked Tool Test

This test was developed by Simon Johns, a PhD student in ACCIS, University of Bristol. In this test, the tool made of aluminium was linearly scratched at every 100 mm. The specimens were placed on the tool carefully so that the length of the specimens were perpendicular to the scratches on the tool. During the curing process, the resin flows into these lines and makes visible traces on the bottom of the specimen. Thereafter, cured specimens were placed on the tool again at their original positions and the shift between the original scratches on the tool and the traces of them on the bottom of the part were measured. In the image given in Fig. 2.2, the original scratches on the tool and the traces of them on the part can be seen clearly.

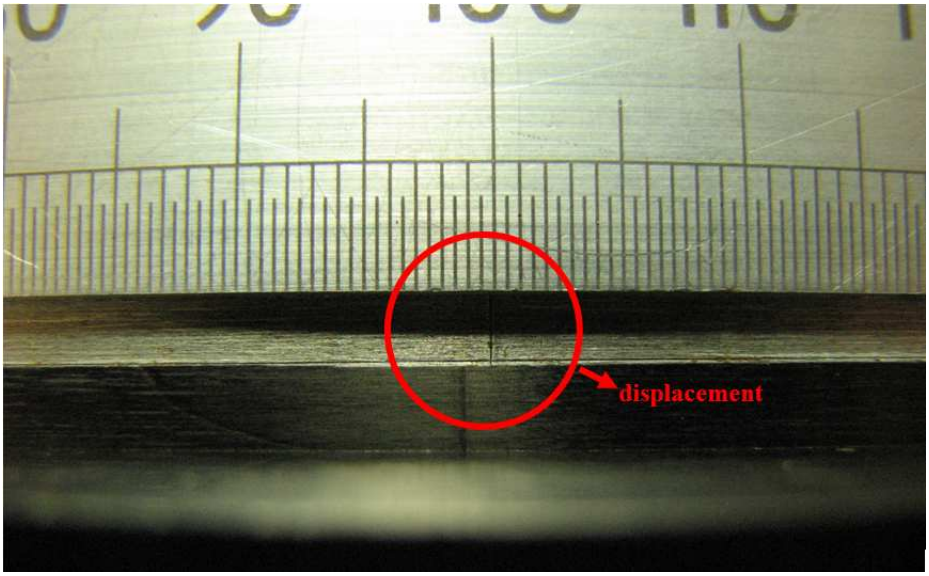

Figure 2.2. Displacement measurements by using marked-tool

2.4. Tension Test

In this test, a single uncured ply of 1 m long and 50 mm wide was placed between the grips of a 100 kN Instron Servohydraulic tensile testing machine. To achieve this, both ends of the ply were reinforced by sandwiching each end between two additional pieces of prepreg, each 50 mm long and 50 mm wide. Then the ends were covered with release film and cured by placing a heating block on it for 10 minutes at 200° C. During this process, the sample was insulated from the bottom by a piece of honeycomb covered with a layer of teflon film.

Then the testing was carried out in a universal testing machine under displacement control at 1 mm/min and load and displacement data was recorded. The strips were loaded up to 500N and this corresponds to a stress of a 80 MPa for 50 mm wide strip of 0.125 mm thick prepreg. Unless specified, all tests were performed at room temperature and the displacement is measured by crosshead movement.

2.5. Preparation of Samples for Image Analysis

In order to observe the relative displacement of the plies and the deformation of the lay-up under the optic microscope, 1x1 cm samples was removed from the corners of both ends of the cured specimen using a water cooled rotary diamond saw. But the preparation for this analysis starts before curing. After finishing lay-up of plies carefully, both ends of the uncured specimen should be trimmed. So the ends of all specimens were cut by a rasor blade with the help of a simple clamping system. The end of the specimen was placed between the grips of the clamp and fixed. To prevent damaging of the fibers on the grip area by the pressure applied on them, additional plies were put on the top and bottom of the ends and the grips were closed not under the full force, but enough to prevent it moving. Nearly a piece of 2 mm was removed from the end by using a sharp blade.

The samples cut from the cured specimen were then placed in a cylindrical mould after applying release agent. Once labeled, the resin and the hardener, mixed in a 4:1

ratio, were poured into the mould, over the corner portion. This moulding resin was left to cure for 24 hours; then the potted sample was polished using a water cooled polishing wheel and grit paper with incrementally decreasing grit sizes from 180 to 1200. Grinding at grit size 180 was performed until the surface of interest was flat; polishing at all other grit sizes was performed until the markings from the previous stage were no longer visible. Finally, samples were polished first by 3 and then by 1 micron diamond suspension for 10 minutes and 0.05 micron alumina for min 15 minutes, samples were washed in the ultrasonic bath using distilled water for 5 minutes after each step.

After the specimens had been polished, they were investigated under the NIKON LV150 optic microscope at a zoom ratio of 50×.

3. FINITE ELEMENT METHOD

3.1. Material Properties

During an actual autoclave process, firstly the material is in the viscous state. The composite cannot sustain any transverse stress, whereas it can sustain some fibre stresses. Although the shear modulus of the resin is practically zero, due to fibre friction the shear stresses arising from tool interaction or interply slip can be transferred in the through-the-thickness direction. The autoclave pressure is applied, the rigid mould, which may also impose tool interaction forces, supports the composite. Consolidation takes place as the voids are suppressed, expelled from the composite, and extra resin bleeds.

Then, the resin goes through the rubbery state, defined by a characteristic value of the rubbery modulus of the resin. The cure shrinkage takes place at this step.

Finally, the resin vitrifies and transforms to the glassy state, and resin modulus increases a few orders of magnitude. The deformations imposed in the rubbery state are frozen in and as the autoclave pressure and restraints imposed by the mould are removed by removing the boundary conditions, the part is allowed to deform freely as it cools down to room temperature.

These considerations suggest that the process should be modeled in three steps: viscous, rubbery, and glassy. The analysis is based on a number of simplifying assumptions, most of which are reasonable. Vitrification is treated as a point at which the material suddenly changes from the rubbery to glassy state with constant properties in each case. To treat this with full viscoelasticity would greatly increase the complexity of the analysis and the amount of material data required, which is difficult to obtain. Assuming fully relaxed properties until an appropriately chosen vitrification point is a pragmatic approach and is argued to be a valid simplification. The viscous state is represented in Step-1, rubbery state in Step-2 and glassy state in Step-3. In a previous

study [23], the properties of AS4/8552 composite in the rubbery and glassy states were obtained by using a Finite Element Analysis based micromechanics approach. The rubbery and glassy properties are given in Table 3.1. Since there is no data regarding the viscous state, rubbery properties are used in this state.

3.2. Solution Steps

The viscous state is represented in Step-1, rubbery state in Step-2 and glassy state in Step-3. Although the Finite Element Model is implemented as a 3-Step Model, the material properties used in Step-1 and Step-2 are the same, since there is no data about the viscous properties of the material. However, since it is known that significant fibre stresses develop due to tool-part interaction in the viscous state; this state is included into the model as the first state. Initially, the part is at 331.5° C and the tool is at 20° C. A fictitiously high initial temperature is assigned to the part to account for the 0.45 percent cure shrinkage in the rubbery state as the part cools from 331.5 to 180° C in Step-2. There is an autoclave pressure of 0.689 MPa on the bag surface of the part. In Step-3, the tool and part cools down to 20° C so that the part becomes glassy. The applied pressure is removed and the part is separated from the tool and spring-in and warpage develops.

3.3. Elements

8-node biquadratic quadrilateral generalized plane strain elements are used. The generalized plane strain theory used in ABAQUS assumes that the model lies between two bounding planes, which may move as rigid bodies with respect to each other, thus causing strain in the direction perpendicular to the plane of the model. It is assumed that the deformation of the model is independent of position with respect to this direction, so the relative motion of the two planes causes a direct strain in the direction perpendicular to the plane of the model only. The elements are defined with a reference node, and restraining this node gives a plane strain condition whereas setting it free gives a plane stress condition.

In the FEA model, a common reference node is defined for both the tool and the part in Step-1 and Step-2. This reference node is restrained for rotation so that the two bounding planes are free to displace but do not rotate with respect to each other. This allows the thermal expansion effect of the tool perpendicular to the plane of the model to be taken into account, and preventing the spread of the composite in viscous or rubbery states under the autoclave pressure. Upon vitrification, the modulus increases and the restraints imposed by the tool cease to be effective. The tool is removed from the model in Step-3, and the part section is now in a plane stress condition. The use of generalized plane strain elements allows one to switch from the plane strain condition in the rubbery state to plane stress in the glassy state by removing the restraints on the reference node common to all elements[21].

3.4. Interface Behavior

When developing the FEA models, both the tool/part and interply interactions are considered. In the finite element Model 1 implemented in this study, there is only one contact pair, which is between the tool and the part. In Model 2, however, there are two contact pairs, one of them is between the tool and the ply adjacent to the tool and the other is between the ply adjacent to the tool and the rest of the plies (as a single part). Both contact pairs are active during Step 1 and Step 2, and the tool/part contact is deleted in Step-3, and interply contact is switched to ROUGH in Step-3 to account for ceasing relative motion between plies. Tool/Part and interply interactions are modeled using ABAQUS mechanical contact interaction modeling capabilities. Contact surfaces are defined for interactions, using ABAQUS option *SURFACE, and then these surfaces are matched by using the option *CONTACT PAIR. The characteristics of the contacting surfaces are defined by using the option *SURFACE BEHAVIOR.

Different surface characteristics can be defined by the latter option. Interaction normal to the surface is the default "hard" contact relationship, which allows no penetration of the slave nodes into the master surface and no transfer of tensile stress across the interface. Interaction tangential to the surface is modeled with the classical isotropic Coulomb friction model, where the interfacial shear stress is proportional to

the contact pressure, and the constant of proportionality is the friction coefficient. In addition to this, ABAQUS allows the introduction of a shear stress limit, which is the maximum value of shear stress that can be carried by the interface before the surfaces begin to slide (Fig. 3.1).

The value of 0.2 MPa for $\tau_{t/p}$ is the shear stress measured in [19]. Microscopic observations show that there is relative sliding between the prepreg layers. So $\tau_{p/p}$ should be smaller than $\tau_{t/p}$. Friction coefficients between tool/part and prepreg/prepreg is not very important because sliding friction prevails.

Parameters for interfaces used for modeling interply and tool/part interactions are listed in Table 3.2.

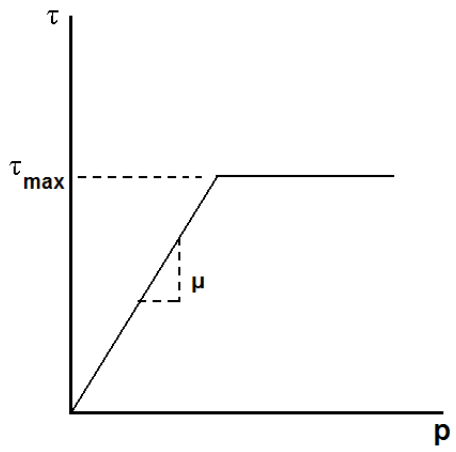

Figure 3.1. Interface friction characteristics

3.5. Meshing and Boundary Conditions

Using ABAQUS, $[0_8]$, $[0_2/90]_s$, $[0_2/90_2]_s$, $[0_2/90_3]_s$ and $[0_2/90_4]_s$ lay-ups are modeled.

The mesh geometries and boundary conditions of the two types of models are shown in Fig. 3.2 to Fig.3.4.

Table 3.1. Composite material properties obtained by micromechanics [23]

		FEBMM	
Property	Unit	Rubbery	Glassy
E_{11}	MPa	132000	134000
$E_{22} = E_{33}$	MPa	165	9500
$G_{12} = G_{13}$	MPa	88.6	4900
G_{23}	MPa	44.3	4900
$\nu_{12} = \nu_{13}$		0.346	0.3
ν_{23}		0.982	0.45
α_{22}			33
ε_{22}^{cure}		0.48	

Table 3.2. Interface parameters

Parameter	**Definition**	**Value**
$\mu_{t/p}$	Friction coefficient between tool/part	0.5
$\mu_{p/p}$	Friction coefficient between plies	0.3
$\tau_{t/p}$	Maximum sliding stress between tool/part	0.2 MPa
$\tau_{p/p}$	Maximum sliding stress between plies	0.1 MPa

3.6. Model 1

Model 1 has two different versions, Model 1-a and Model 1-b.

3.6.1. Model 1-a

The Model 1-a shown in Fig.3.2 has two parts: the tool and the part. The bag surface of the part is placed between the coordinates (0,0) and (500,0). The symmetry line lies in y- axis and passes from (0,0). A reference node is also placed at (0,0). The rotations about x- and y- axis are hindered. The thermal expansion of the tool is defined to be $24.7x10^{-6\circ}C^{-1}$ Only the bottom nodes of the tool are restrained in the vertical direction, and the symmetry line in the horizontal direction. The elements of the tool are indicated in darker gray. The coordinate system show the material orientations in the composite part. The fibers lie along the x- direction in the part with the $[0_8]$ lay up. The material properties in y- and z- directions are the same. In $[0/90]_s$ only in bottom and top plies, fibers lie along x- direction, whereas in the second and third plies the fibers lie along z- direction.

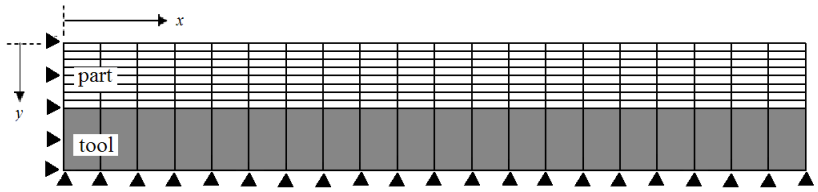

Figure 3.2. Meshing of Model 1-a

The tool-part interaction is defined as a contact behavior without softening. The friction coefficient, $\mu_{t/p}$ is assumed to be 0.5 and maximum shear stress,$\tau_{t/p}$ 0.2 MPa.

3.6.2. Model 1-b

With the interfacial behavior in Model 1-a which can be seen in Fig. 5.10, it is concluded that applying a constant friction boundary condition on the tool surface of the part may be used instead of the tool. It is noted also that the relative slipping is non linear. Model 1-a was then modified so that it does not have the tool in contact

with the part. In this model, instead of tool, the frictional force that can arise due to tool-part interaction is specified. The boundary conditions applied in modified Model 1 is shown in Fig.3.3.

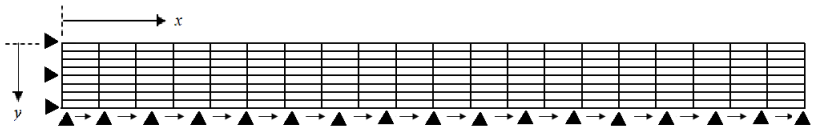

Figure 3.3. Meshing of Model 1-b. Instead of the tool, frictional boundary condition is applied in Step 1.

The initial conditions are only in type of temperature. The part is initially at 331.5° C. In the first step, the temperature of the part decreases to 180° C. A fictitiously high initial temperature is assigned to the part to account for the 0.45 percent cure shrinkage in the rubbery state as the part cools from 331.5 to 180° C. There is also a shear traction of 0.2 MPa on the tool/part interface in second direction, which is considered to be in contact with the tool. In the second step the temperature drops further to 20° C and there is no shear traction. It is expected that the warpage and shear stress gradient tends to be similar to the first model.

3.7. Model 2

Model 2 is developed by considering the interply -interaction. A similar model is used by Twigg et al [13]. According to [13] , it was assumed that, slip also occurs between the plies of the laminate itself in addition to the tool-part interface and for simplicity it is assumed that the sliding friction condition occurs only at two interfaces: between tool and the ply adjacent to the tool and between this ply and the rest of the part. Other assumptions are as follows:

- The laminate is uni-directional and hence the modulus and thermal expansion of each ply is identical [13].
- The interply sliding friction coefficient is smaller than the interface sliding friction coefficient. This is based on experimental evidence presented by Flanagan [17].

The geometry and meshing type of this model, which is shown in Fig. 3.4, is the same as the Model 1. Different than the first model, in the code, there are two contact pairs, one of them is between tool and ply adjacent to the tool and the other one is between the ply adjacent to the tool and the rest of the plies (as a single part). The ply adjacent to the tool -shown in light gray- is separated from the part. The tool is shown in dark gray.

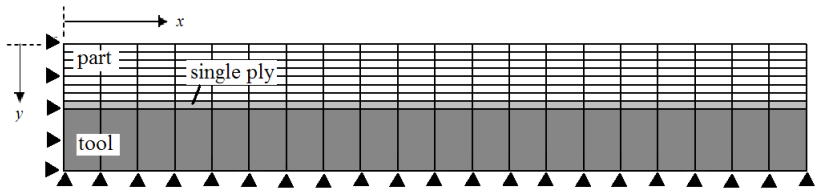

Figure 3.4. Meshing of Model 2

4. ELASTICITY SOLUTIONS

Elasticity solutions were made to compare the results of the two finite element models mentioned above. In the PhD thesis of Arafath [20], a closed-form analytical model based on the theory of elasticity is developed to analyze the process-induced stresses and deformations that develop during the cure cycle of a composite flat part. His attempt was to predict the stress development in a flat composite part laid on a solid tool. He considers this problem is similar to the classical bi-metallic beam under thermal load. The problem he considered is shown in Fig. 4.1.

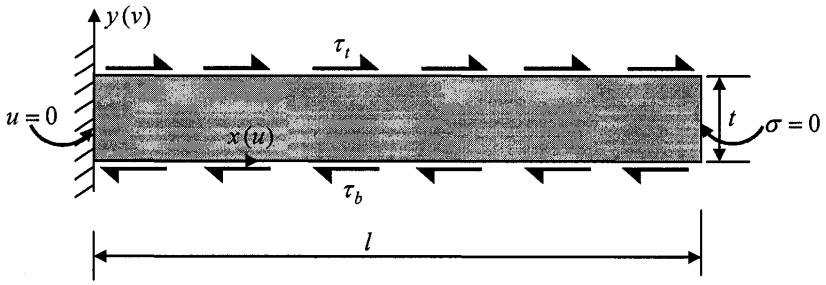

Figure 4.1. Schematic of a beam under applied traction at the top and bottom surface [20]

In his study, calculations were done for a stress free surface at the top and applied shear stress at the bottom, as well as fully bonded case with equal displacements and shear stresses along the length of tool and the part at the interface. In this solution the tool-part interaction is affected by the compliance of the tool.

In this study, calculations were done for the sticking and sliding boundary conditions. In sticking boundary condition a displacement is characterized by the thermal expansion of the tool is prescribed at the interface. In sliding boundary condition a constant shear stress is assigned at the interface.

The equilibrium equation in the x-direction can be written as

$$\frac{\partial \sigma_{xx}}{\partial x} + \frac{\partial \tau_{xy}}{\partial y} = 0 \tag{4.1}$$

The stress-displacement relationship is given below by

$$\sigma_{xx} = E_{xx}\left(\frac{\partial u}{\partial x} - \varepsilon^{ther}\right)\tau_{xy} = G_{xy}\left(\frac{\partial u}{\partial y} + \frac{\partial v}{\partial x}\right) \tag{4.2}$$

where ε^{ther} is the axial free thermal strain and u and v are the displacements in x and y directions, respectively. When we transform the variables

$$\bar{u} = u - \varepsilon^{ther}x$$

So, we can write

$$\frac{\partial \bar{u}}{\partial x} = \frac{\partial u}{\partial x} - \varepsilon^{ther},\ \frac{\partial \bar{u}}{\partial y} = \frac{\partial u}{\partial y} \tag{4.3}$$

Assuming that there is no bending of the beam during the cure cycle and displacement in y-direction is constant, it can be written

$$\frac{\partial v}{\partial x} = \frac{\partial v}{\partial y} = 0 \tag{4.4}$$

when we substitute Eqs. 4.2 and 4.3 into the Eqs.4.1,we get

$$\frac{\partial}{\partial x}\left(E_{xx}\frac{\partial \bar{u}}{\partial x}\right) + \frac{\partial}{\partial x}\left(G_{xy}\frac{\partial \bar{u}}{\partial y}\right) = 0 \tag{4.5}$$

Let the beam is homogeneous,

$$E_{xx}\frac{\partial^2 \bar{u}}{\partial x^2} + G_{xy}\frac{\partial^2 \bar{u}}{\partial y^2} = 0$$

which is a second order partial differential equation. Let

$$\bar{u} = X(x)\,Y(y)$$

and substitute in Eq. 4.5, we get

$$\begin{aligned} &E_{xx}\ddot{X}Y + G_{xy}X\ddot{Y} = 0 \\ &\frac{\ddot{X}}{X} = \frac{-1}{c^2}\frac{\ddot{Y}}{Y} = \chi \end{aligned} \tag{4.6}$$

where

$$c = \sqrt{\frac{E_{xx}}{G_{xy}}}$$

The solution of Eq. 4.6 depends on the value of χ. The only solution which satisfies the boundary conditions is

$$\chi = -k^2$$

when

$$\chi < 0$$

.

Now, an eigenvalue problem given below is obtained

$$\begin{aligned} \frac{\ddot{X}}{X} &= \frac{-1}{c^2}\frac{\ddot{Y}}{Y} = -k^2 \\ \ddot{X} + k^2 X &= 0 \\ \ddot{Y} - \beta^2 Y &= 0 \end{aligned} \tag{4.7}$$

where

$$\beta = ck$$

is a diffusion-like coefficient as is commonly referred to in shear-lag analysis [20].

The general solution for the two ordinary differential equations in Eq. 4.7 is

$$\begin{aligned} X &= A_1 \cos(kx) + B_1 \sin(kx) \\ Y &= A_2 e^{\beta y} + B_2 e^{-\beta y} \end{aligned} \tag{4.8}$$

When we apply the boundary conditions given as

$$\text{at } x = 0 \; u = 0 \Rightarrow A_1 = 0$$

$$\text{at } x = L \; \sigma_{xx} = 0 \Rightarrow \cos(kL) = 0 \Rightarrow k = k_n = \frac{(2n-1)\pi}{2L}$$

we obtain the displacement, normal stress and shear stress in the infinite series form given below

$$
\begin{aligned}
u &= \sum_{n=1}^{\infty} \left\{ \sin\left(k_n x\right) \left(A_{2n} e^{\beta_n y} + B_{2n} e^{-\beta_n y} \right) \right\} + \varepsilon^{ther} x \\
\sigma_{xx} &= \sum_{n=1}^{\infty} \left\{ E_{xx} k_n \cos\left(k_n x\right) \left(A_{2n} e^{\beta_n y} + B_{2n} e^{-\beta_n y} \right) \right\} \\
\tau_{xy} &= \sum_{n=1}^{\infty} \left\{ G_{xy} \beta_n \sin\left(k_n x\right) \left(A_{2n} e^{\beta_n y} - B_{2n} e^{-\beta_n y} \right) \right\}
\end{aligned}
\tag{4.9}
$$

When we solve Eq. 4.9 for the sticking case, the BC' s given in Fig. 4.2 below are applied

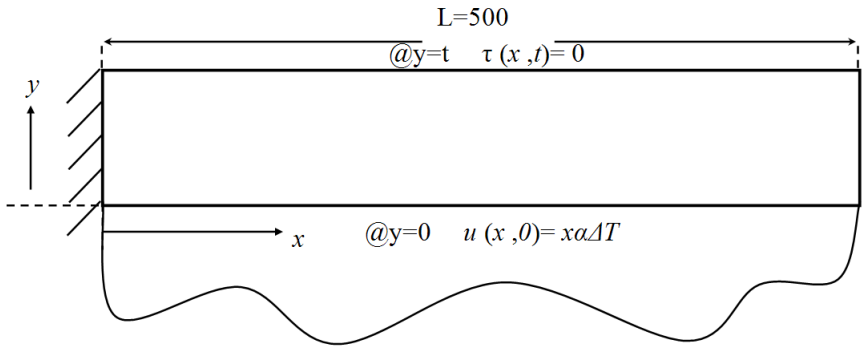

Figure 4.2. Sticking boundary conditions

$$
\begin{aligned}
u\left(x,0\right) &= x\alpha\Delta T \quad @\, y = 0 \\
\tau\left(x,t\right) &= 0 \qquad\qquad @\, y = t
\end{aligned}
\tag{4.10}
$$

The coefficients A_{2n} and B_{2n} are found as

$$
\begin{aligned}
A_{2n} &= \frac{\Delta T \alpha \left(-1\right)^{n+1}}{\left(1 + e^{2t\beta_n}\right) k_n^2} \\
B_{2n} &= \frac{e^{2t\beta_n} \Delta T \alpha \left(-1\right)^{n+1}}{\left(1 + e^{2t\beta_n}\right) k_n^2}
\end{aligned}
\tag{4.11}
$$

When we consider sliding case, the BC's given in Eq. 4.12 are applied Fig. 4.3.

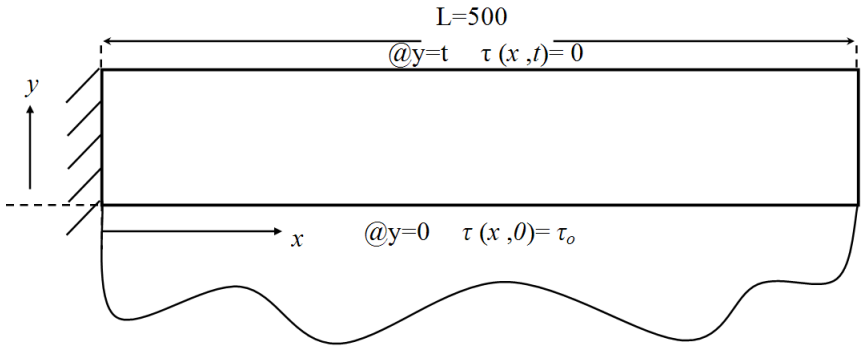

Figure 4.3. Sliding boundary conditions

$$\begin{aligned} \tau_{xy}(x,0) &= \tau_o \quad @\, y = 0 \\ \tau_{xy}(x,t) &= 0 \quad @\, y = t \end{aligned} \tag{4.12}$$

We get the coefficients as given in Eq. 4.13 for the sliding case.

$$\begin{aligned} A_{2n} &= \frac{2\tau_o e^{-2\beta_n t}}{k_n L G_{xy} \beta_n \left(e^{-2\beta_n t} - 1\right)} \\ B_{2n} &= \frac{2\tau_o}{k_n L G_{xy} \beta_n \left(e^{-2\beta_n t} - 1\right)} \end{aligned} \tag{4.13}$$

A_{2n} and B_{2n} are put into the Eq. 4.9 to find the solution. since only the tool-part interactions in the rubbery state are investigated using the closed-form elasticity solutions, rubbery material properties given in Table 3.1 are used.

5. RESULTS AND DISCUSSION

5.1. Model 1

When we compare the results for the models with and without tool the results are pretty same. For example for a 500 mm long part, at the cross-section at 400 mm the stress distribution is almost the same, which reveals that the second model is good enough to reflect the effects of the tool. In Model 1-b, instead of the tool, frictional boundary condition is applied in Step-1 and 2. A complex model with tool is not needed to show the effects of the tool. The similarity of the results can be seen below in Figs. 5.1 and 5.2. In Fig. 5.2, the results of warpage fall onto each other.

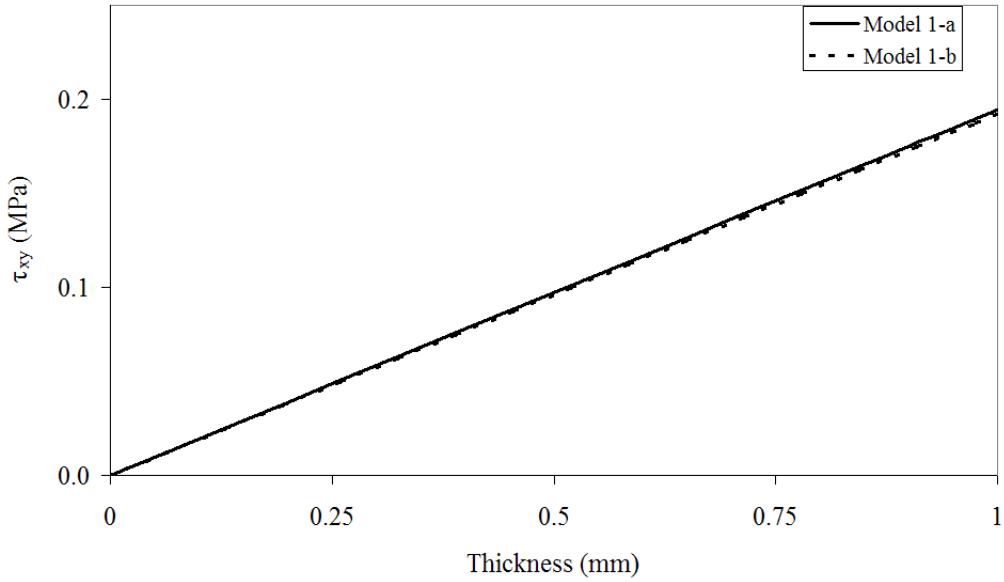

Figure 5.1. The comparison of the shear stress distribution through the thickness for Model 1-a and Model 1-b.

Fig. 5.3 shows the warpage of the half of the composite part of 1 m length for Model 1 and 2. Model 1 gives very small distortion and hence is inadequate in capturing the warpage behavior of the parts manufactured in the experimental part of this study. Model 2 gives a parabolic, concave-up warpage which represents the sense of bowing of the manufactured parts.

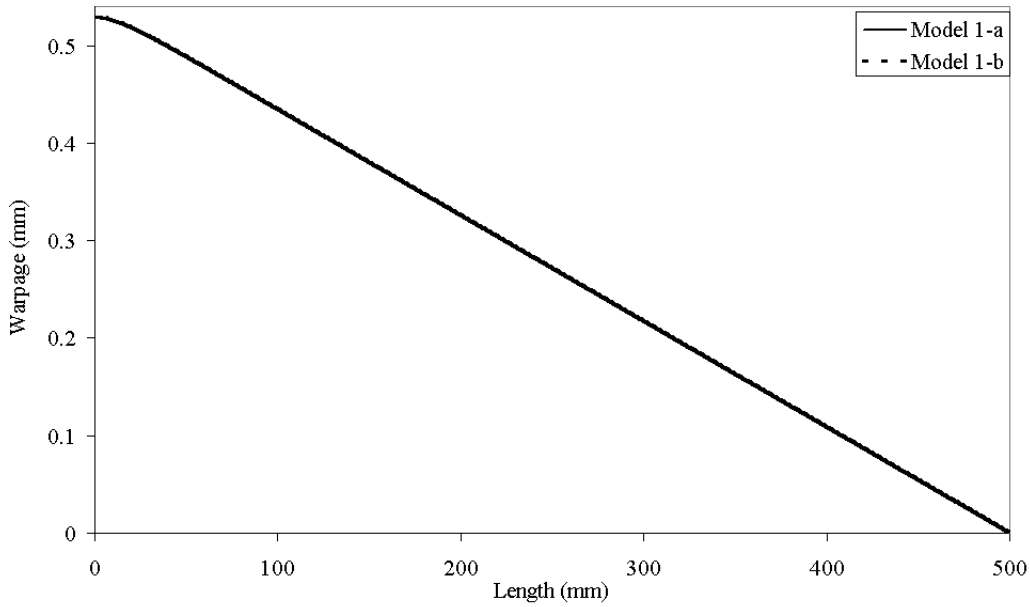

Figure 5.2. The comparison of the for Model 1-a and Model 1-b.

The reason for Model 1 not capturing the warpage observed is the fact that the FE model does not give a fibre direction stresss gradient through the thickness. This can be seen in Fig. **??** where the fibre stresses are plotted along the length of the part at the tool and bag sides. There is a stress gradient only at a small region close to the symmetry line. So the warpage is restricted to this small region, and the rest of the part does not warp when removed from the tool.

Fig. 5.5 and Fig. 5.6 show the shear stress distribution and the stress distribution in the fibre direction respectively for $[0_8]$ parts of Model 1 at the end of Step-2. There is a through-thickness shear stress gradient in the part, except the symmetry line. The shear stress decreases from a value of 0.2 MPa to 0(zero) MPa as moving from the tool side to the bag side of the part, which shows that the shear stress is distributed linearly through the thickness of the part as expected.

The stress distribution in x-direction, which is indicated as σ_{xx} shows no gradient through the thickness at regions away from the symmetry line. But it increases towards the symmetry line. Fig. 5.6 shows σ_{xx} values at different cross-sections along the half length of the 1 m long part.

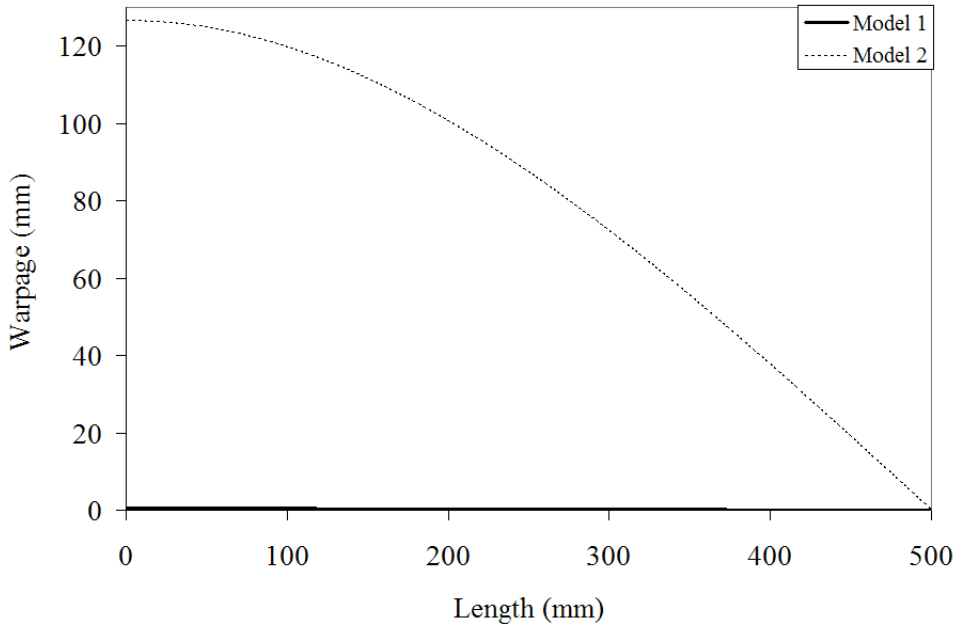

Figure 5.3. Models 1 and 2 predictions of warpage for a 1 m long part with $[0_8]$ lay-up along its half length at the end of Step-3.

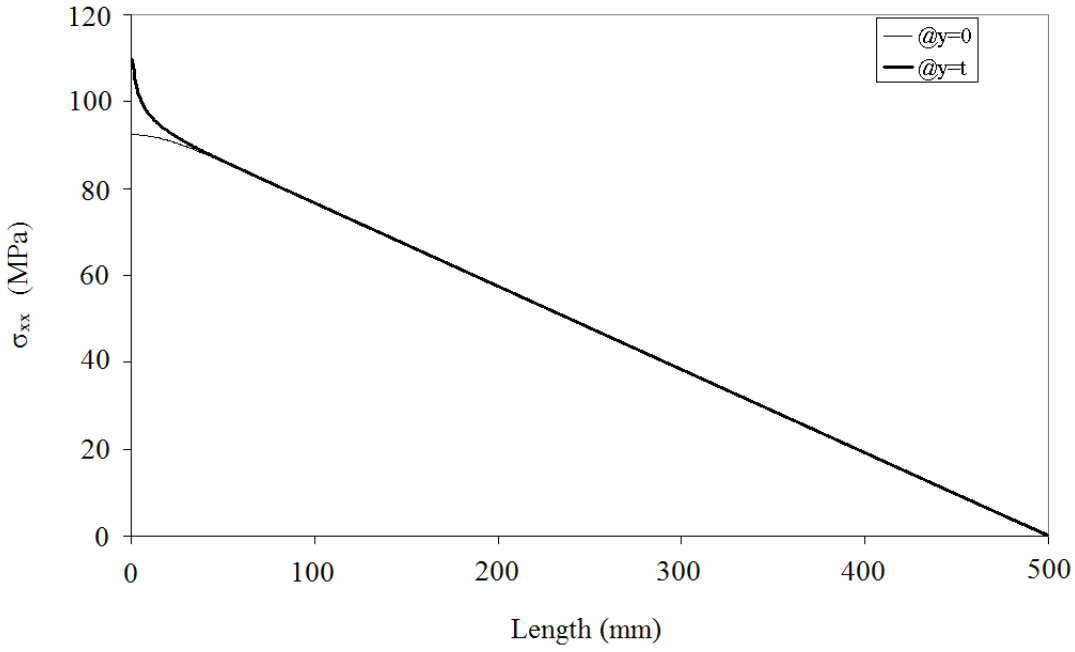

Figure 5.4. Stress in the fibre direction for $[0_8]$ lay-up at the tool and bag side at the end of Step-2 increases towards the symmetry line.

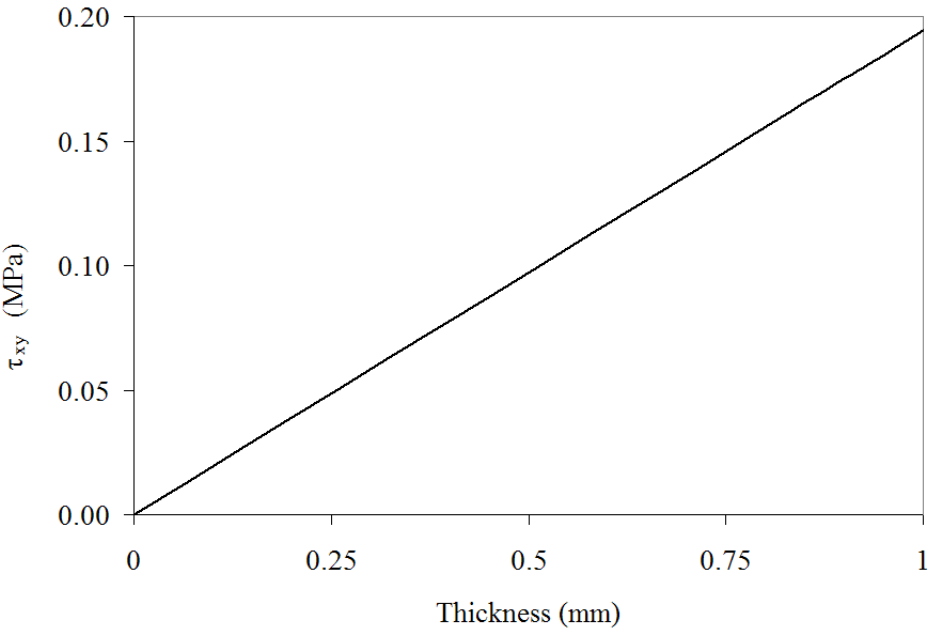

Figure 5.5. Model 1 predictions of shear stress gradient at x=250 mm at the end of Step-2 along the half length of 1000 mm long [0_8] part .

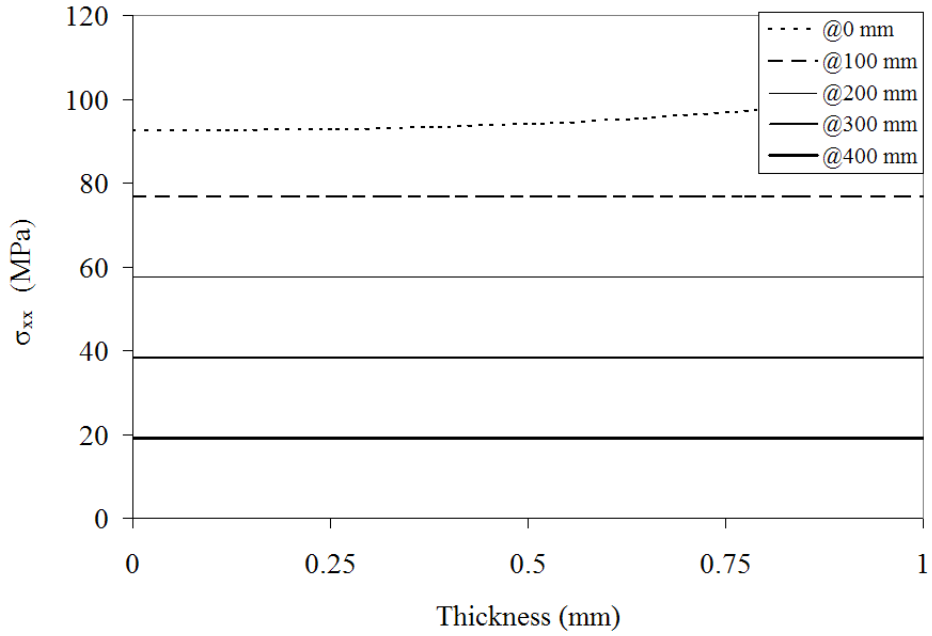

Figure 5.6. Model-1 predictions for fibre direction stress distribution in x-direction at the end of Step-2 for [0_8]-orientation.

For the part with the orientation of $[0_2/90_2]_s$, the warpage is greater than that with the orientation of $[0_8]$, which is shown in Fig. 5.7. In Fig. 5.8 shear stress at the end of Step-1 is plotted at five cross- sections for a 500 mm long part. The values are almost the same at every cross- section except at symmetry line, so that the lines for cross-sections at 100, 200, 300 and 400 mm. overlap in the figure. There is a stress gradient in the bottom and top plies, whereas the gradient is minimal in the 90° plies in which the fibers lie along the third direction.

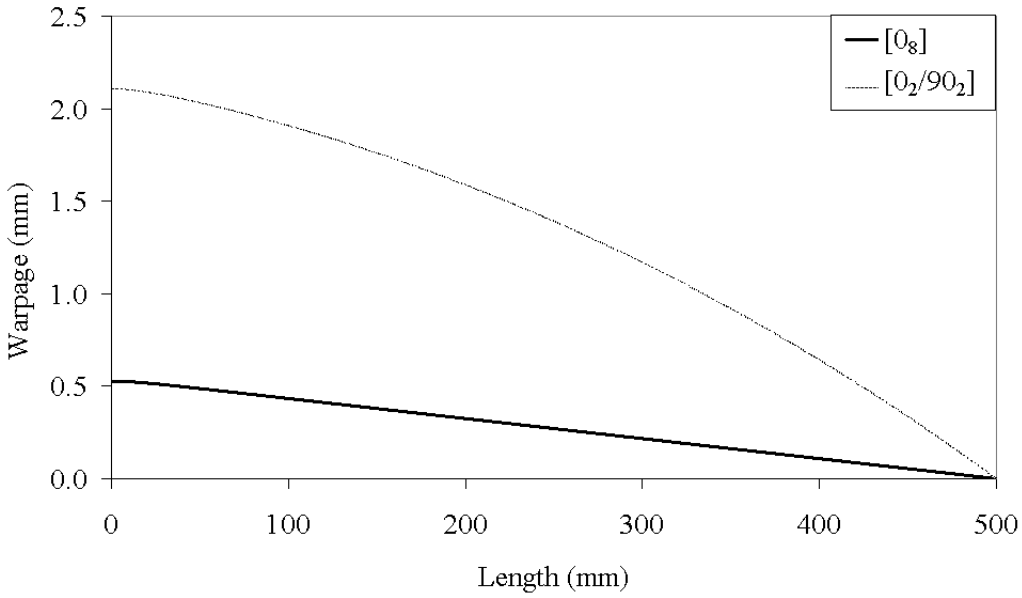

Figure 5.7. Model 1 predictions of warpage for $[0_8]$ and $[0_2/90_2]_s$-orientations.

In Fig. 5.9 the stresses in fiber direction are plotted at 5 cross-sections at the end of the first step. Plies with 90-orientation carries no stress, whereas the stress increases towards the symmetry line. The strain values are nearly zero in z-direction.

No gradient of stress is observed from the tool side to the bag side of the part, but there is an increase of σ_{xx} values towards the symmetry line of the part.

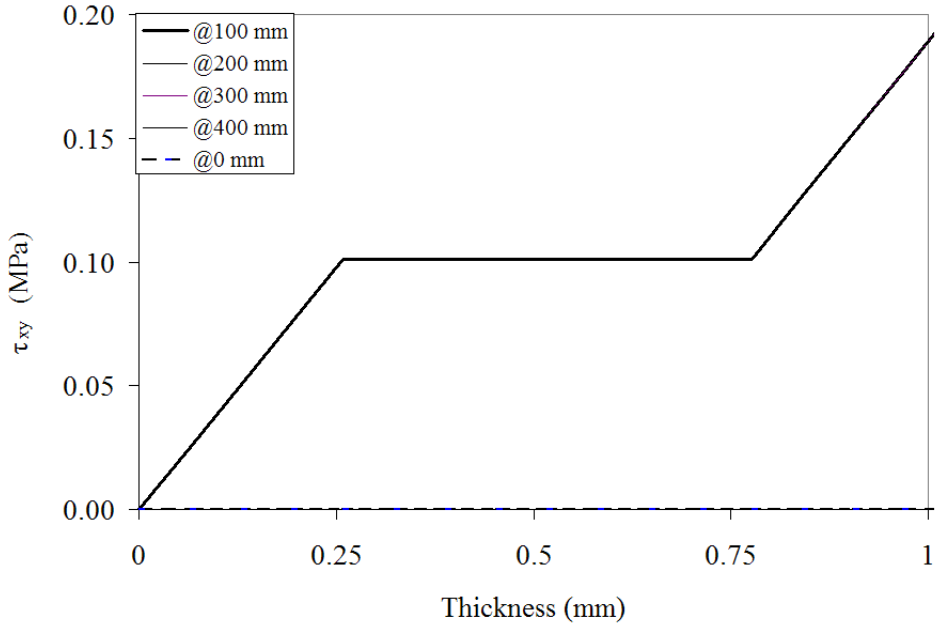

Figure 5.8. Model 1 predictions for τ_{xy} at the end of Step-2 for 1 m long part at three different cross-sections (at 0mm (symmetry line), 100mm, 200mm, 300mm, 400mm for $[0_2/90_2]_s$-orientation .

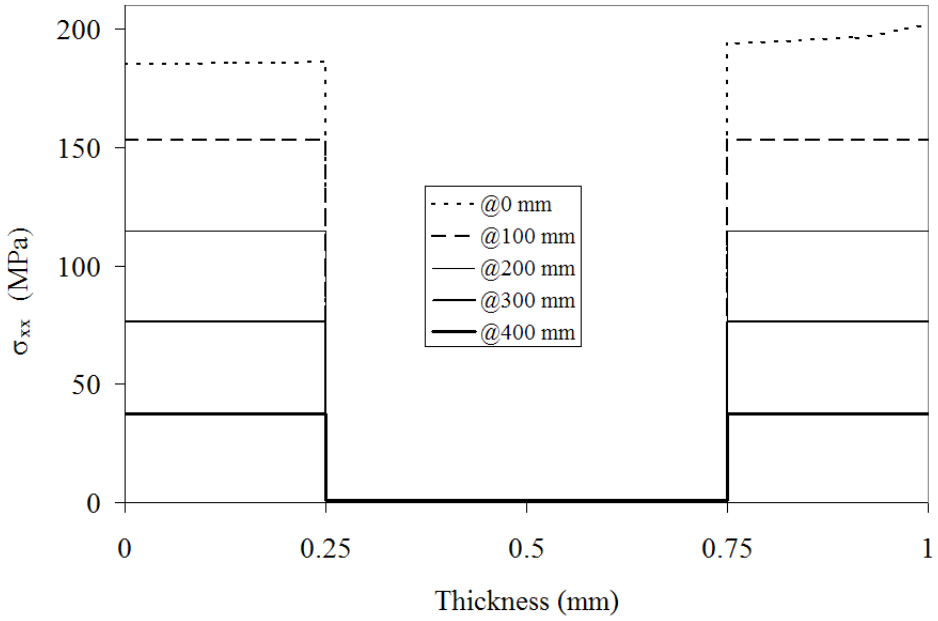

Figure 5.9. Model 1 predictions of through-thickness stress distributions in x-direction at the end of Step-1 for $[0_2/90_2]_s$ lay-up.

In Fig. 5.10, contact pressure (CPRESS), contact opening (COPEN), contact shear stress (CSHEAR) and relative slipping (CSLIP) at the tool-part interface are plotted. It can be seen that the contact shear stress is almost constant along the length of the part, except there is only a small region (0-1.25 mm length of the part) where sticking condition prevails and the shear stress has a sharp decrease from 0.2 MPa to 0.05 MPa. Elsewhere sliding with constant maximum shear stress of 0.2 MPa occurs.

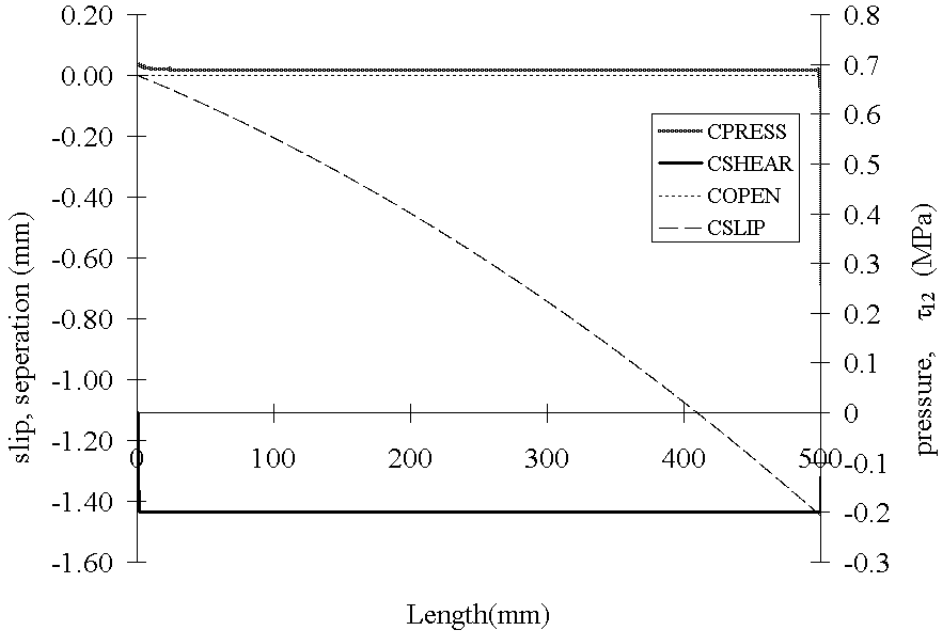

Figure 5.10. Model-1 interface stresses and displacements between tool and part at the end of Step-2.

5.2. Model 2

In Model 2, the tool/part interaction is as in Model-1. Additionally, there is an interaction between the ply adjacent to the tool and the other plies. The maximum shear stress between the tool and the part is fixed at 0.2 MPa. Two different values for the maximum interply shear stress are assumed to be 0.1 and 0.15 MPa in order to observe the effect of the magnitude of the maximum interply shear stress on the overall deformation pattern. The parabolic behavior is better represented than the Model 1. However, the warpage depends greatly on the magnitude of the maximum interply shear stress. The difference is shown in Fig. 5.11. The gradient in shear stress becomes bilinear through the ply adjacent to the tool in Model 2, whereas it is linear in Model 1 (Fig. 5.12).The values $\tau_{t/p}$ and $\tau_{p/p}$ are the maximum shear stresses that these interfaces can carry. There is a discontinuity in σ_{xx} between the ply adjacent to the tool and the rest of the plies. The fibre stress distributions cause a net bending moment which gives the curvature of the strip when it is released from the tool. These can be seen in Figs. 5.13-5.14.

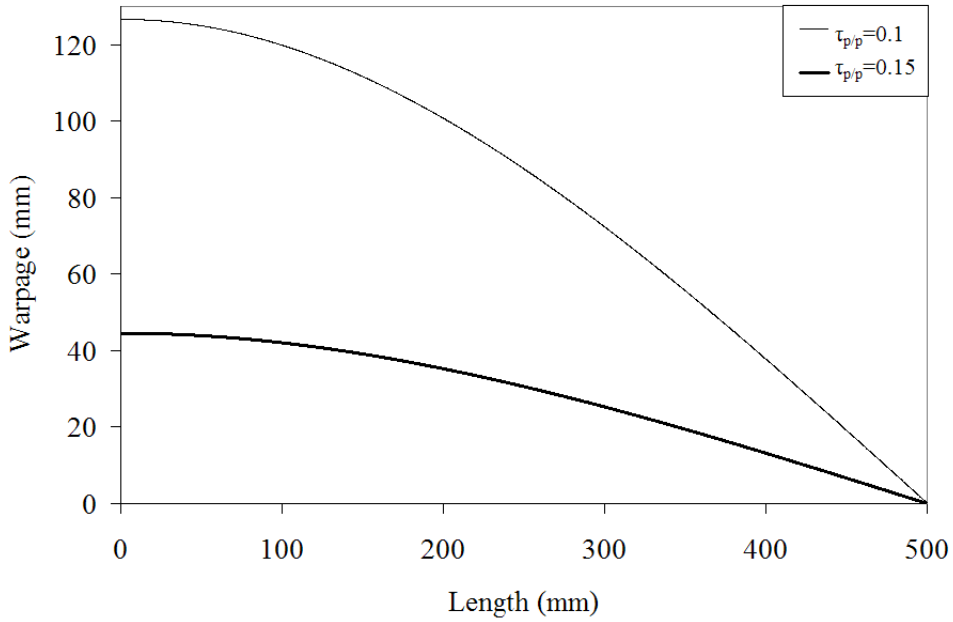

Figure 5.11. Model 2 predictions of the warpage of the $[0_8]_s$ part along its length at the end of Step-3 for two different values of maximum interply shear stress for 1 m long part.

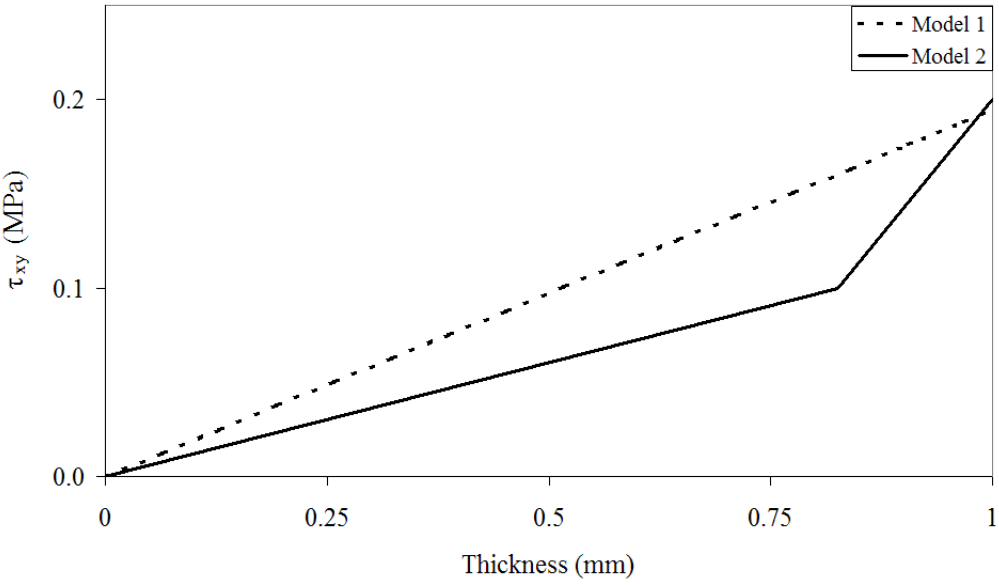

Figure 5.12. Comparison of through thickness shear stress gradient in Model 1 and 2 for 1 mm long part when $\tau_{p/p}$=0.1 MPa and $\tau_{t/p}$=0.2 MPa.

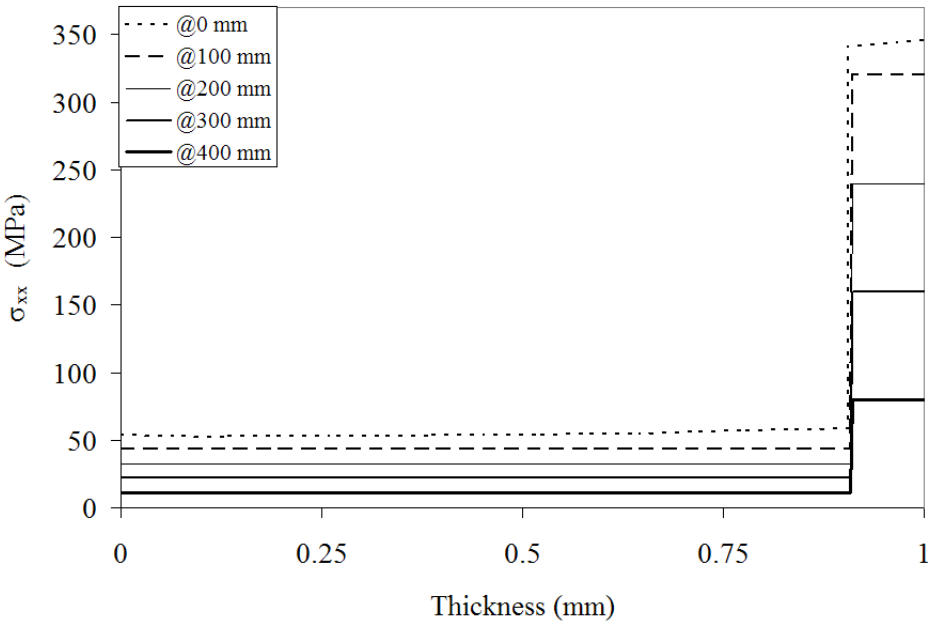

Figure 5.13. Model 2 Through-thickness stress distribution in 2-direction at the end of Step-1 for $[0_8]_s$ part.

In Figs. 5.15 and 5.16, contact pressure (CPRESS), contact opening (COPEN), contact shear stress (CSHEAR) and relative slipping (CSLIP) at the tool-part interface and at the interface between the ply adjacent to the tool and the rest of the part are plotted. In Model 2, contact shear stress remains almost constant along the length of the part in both interfaces and interplies, implying that sliding condition prevails. There is a decrease in shear stress only in a small region of the part towards the symmetry line where the interfaces are sticking.

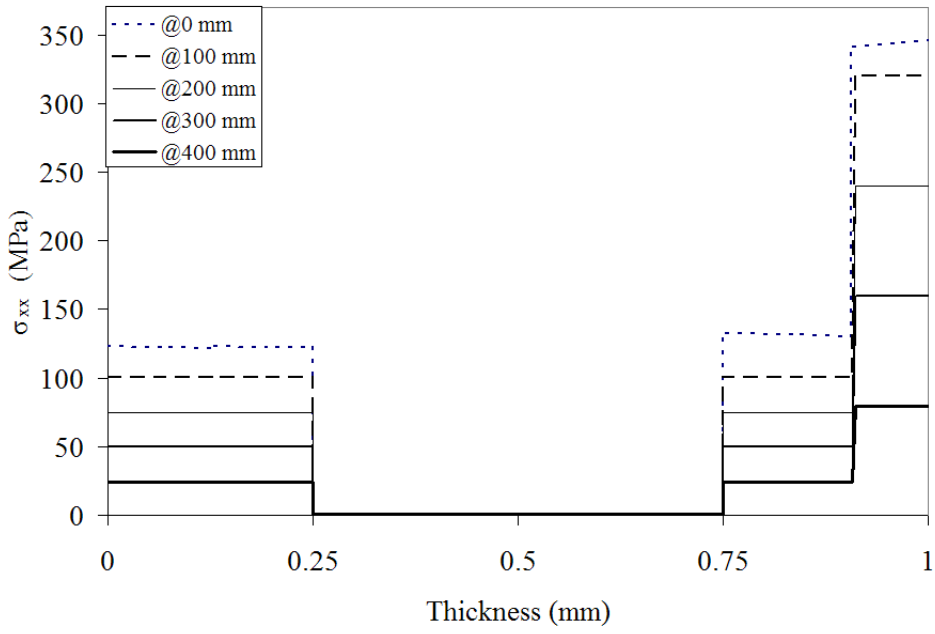

Figure 5.14. Model 2 Through-thickness stress distribution in 2-direction at the end of Step-1 for $[0_2/90_2]_s$-lay-up.

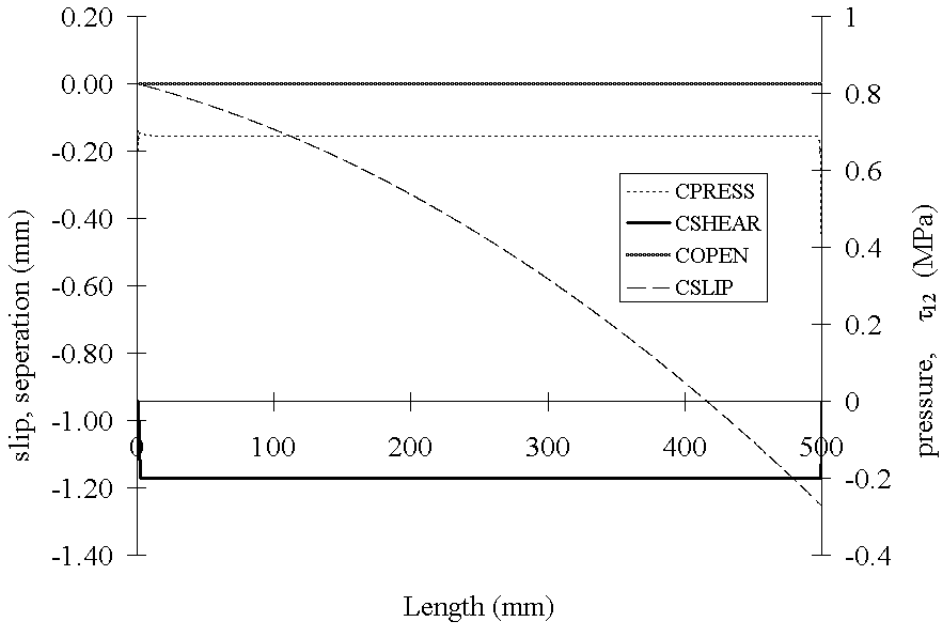

Figure 5.15. Model 2 interface stresses and displacements between tool and part at the end of Step-1.

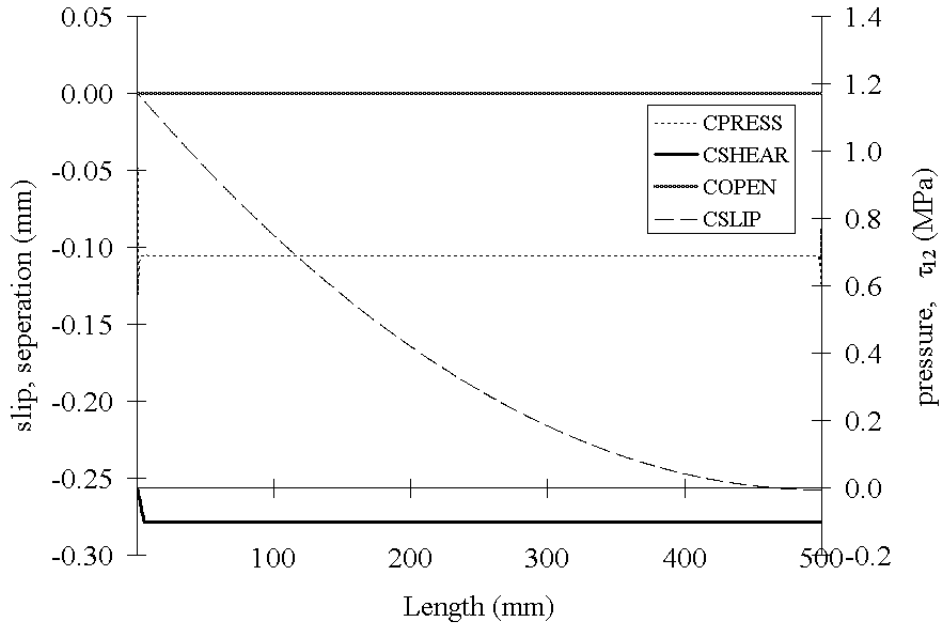

Figure 5.16. Model-2 interface stresses and displacements between the ply adjacent to the tool and the rest of the plies at the end of Step-1.

5.3. Elasticity Solutions

The normal stress in x-direction, σ_{xx} vs. thickness of the part for the sticking boundary conditions is plotted in Fig. 5.17 using Eq. 4.9 with the coefficients in Eq. 4.11. In these equations, ΔT equals to 160° C.

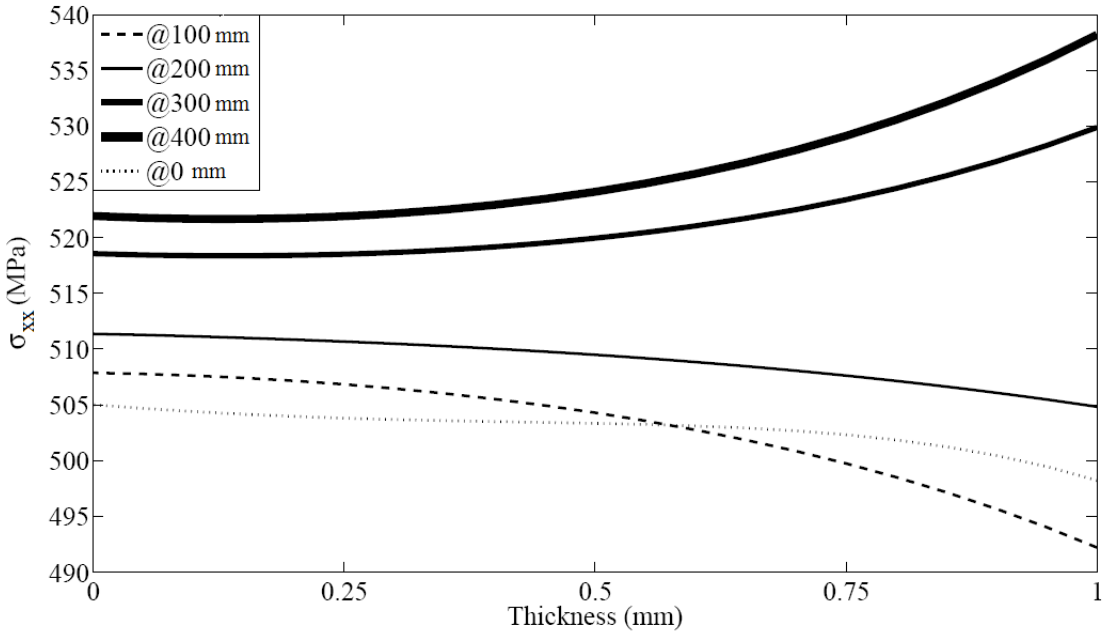

Figure 5.17. Infinite series solution with sticking boundary conditions for a 1 mm thick part

The normal stress in x-direction, σ_{xx} along the thickness of the part for the sliding boundary conditions is plotted in Fig. 5.19 using Eq. 4.9 with the coefficients in Eq. 4.13. Here, τ_o is equal to $\tau_{t/p}$, which is 0.2 MPa and t is equal to 1 mm. If only a single ply is considered, $\tau_o = \tau_{t/p}$ - $\tau_{p/p}$ equals to 0.1 MPa and t equals to 0.125 mm.

When we compare Fig. 5.6 and 5.13 with Fig. 5.18 and 5.19, respectively, it can be seen that the finite element model results are well in agreement with the closed form solutions solved for sliding boundary conditions. Closed- form solutions for the sticking boundary conditions shown in Fig. 5.17 gives very high values of σ_{xx} as compared to the analytical models for a 1 mm thick part.

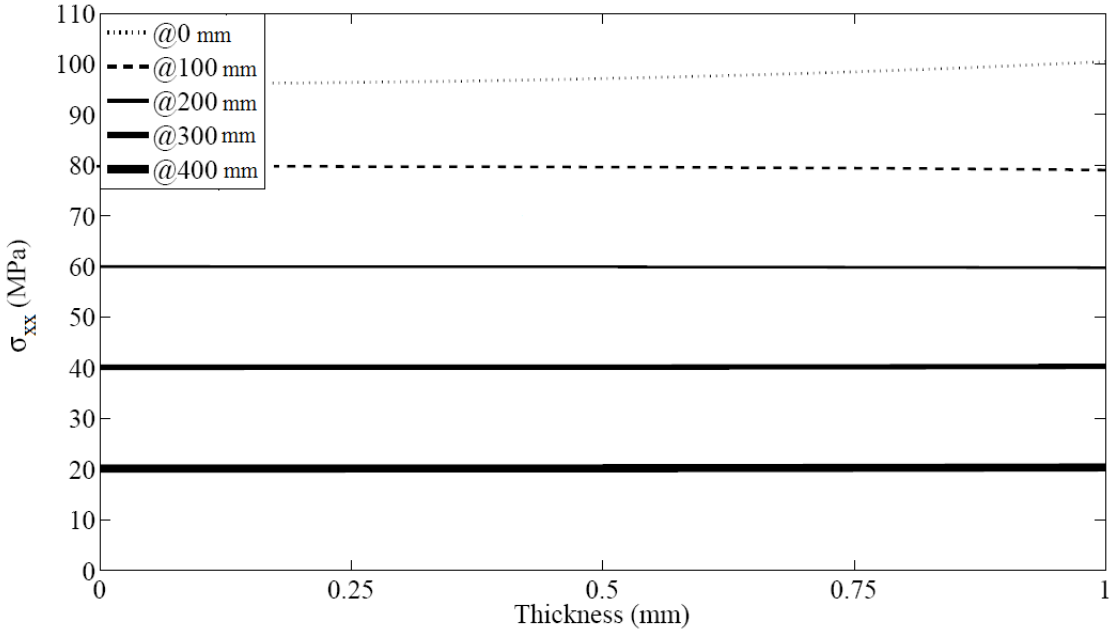

Figure 5.18. Infinite series solution with sliding boundary condition for a 1 mm thick part

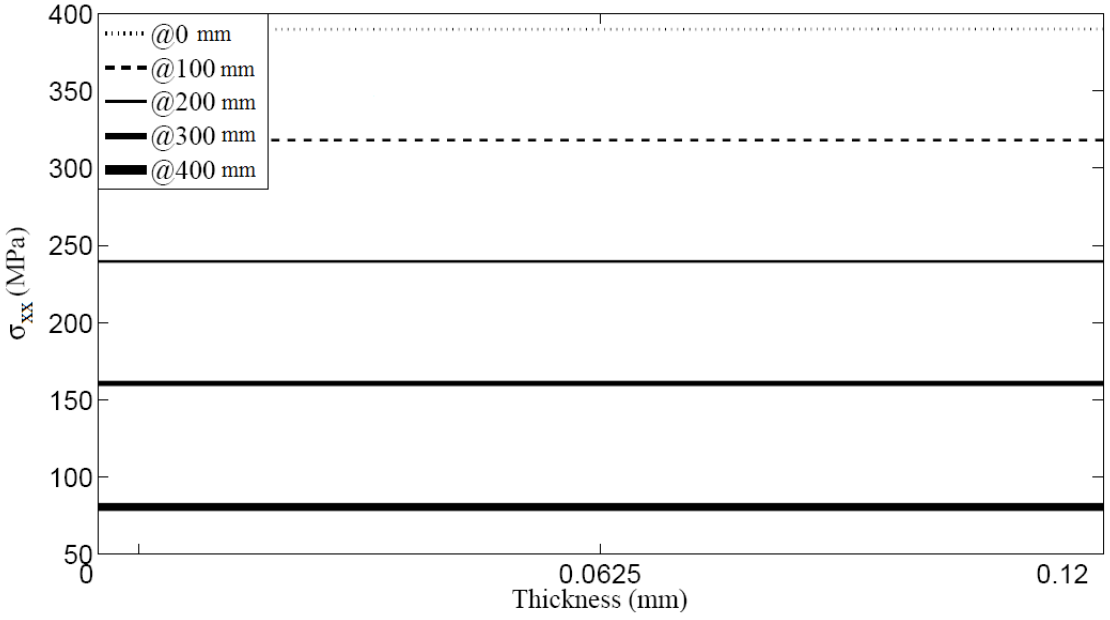

Figure 5.19. Infinite series solution with sliding boundary condition for a 0.125 mm single ply

6. EXPERIMENTAL RESULTS

6.1. Tension Test

The data obtained from the Instron universal testing machine were recorded and then converted into stress-strain diagram. A typical stress-strain diagram is plotted in Fig. 6.1. At the beginning of the curve, a region with a very small slope can be observed. It is accepted that this region represents the initial waviness of the fibers. As the prepreg starts to be pulled, firstly these curvy fibers get linear and then they begin to carry the load applied on them. After this region, the curve increases linearly from which the elastic modulus can be calculated. The curve of unloading does not go back to the zero strain because of the initial stretching effect. No slipping was observed in the gripping area. The initial displacement is calculated as 0.01 mm and this value is added to the results of Model 2 for the$[0_8]$ specimen shown in Fig. 6.2. This is the displacement without causing any fibre stress in the part. In the results obtained in marked-tool test do not include the initial displacemet of the fibres. So, to correct the total displacement caused by the normal stress, the initial displacement should be added to the results of the models.

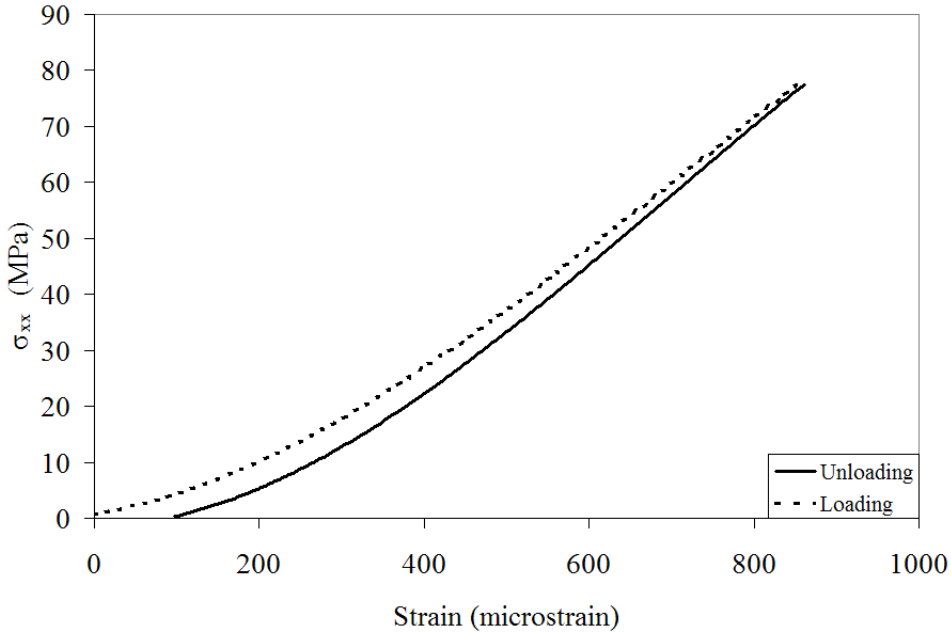

Figure 6.1. Tensile test result for a single ply of 0.125 mm thick

6.2. Marked Tool Test

In Figs. 6.2-6.6 the displacements vs. half length of the part are plotted for 1 m long specimens with various lay-ups. Experimental results are obtained by measuring the difference between the scratches of the tool and the lines on the part as shown in Fig. 6.7. The thermal expansion of the tool is calculated by the Eq.

$$\delta = \alpha x \Delta T$$

The first thing to observe is that the marks on the part is very close to the displacements caused by the thermal expansion of the tool. This suggest that the fibres close to the tool/part interface may stick to the tool surface streched by the tool expansion causing high fibre stresses. However this stress may decay steeply due to high intraply shearing. This hypothesis is also supported by the micrographs taken from the ends of the strips manufactured where both inerply and intraply shearing can be observed (Fig. 6.7-6.9)

Model 1 and Model 2 results are taken from the displacements of the nodes of the part which are in contact with the tool. For the specimens with $[0_8]$ and $[0_2/90_2]_s$ lay-ups (Fig. 6.2 and 6.4) results of Model 2 with two different values for maximum interply shear stress, $\tau_{p/p}$, are plotted. When $\tau_{p/p}$ increases, the results of Model 2 get closer to the results of Model 1. The results of the model and mathematical calculations lies below the experimental results. When the initial stretching was added to the constant shear stress in Fig. 6.4, the values are getting closer to the experimental results although the improvement is minimal and doesn't explain the large discrepancy between the model predictions and experimental values. Since the part was placed straightly on the tool for photographing, the effect of bending moment is eliminated. In that case, the difference between the two curves exists through retraction of the part after removing the part from the tool. When we compare the two models, the model with the separated ply (Model 2) gives closer results to the experiments. This means that assuming the first ply sticks to the tool during the curing process and the remaining plies slide over it is a better approach than considering the part moves as a whole body as modeled in Model 1.

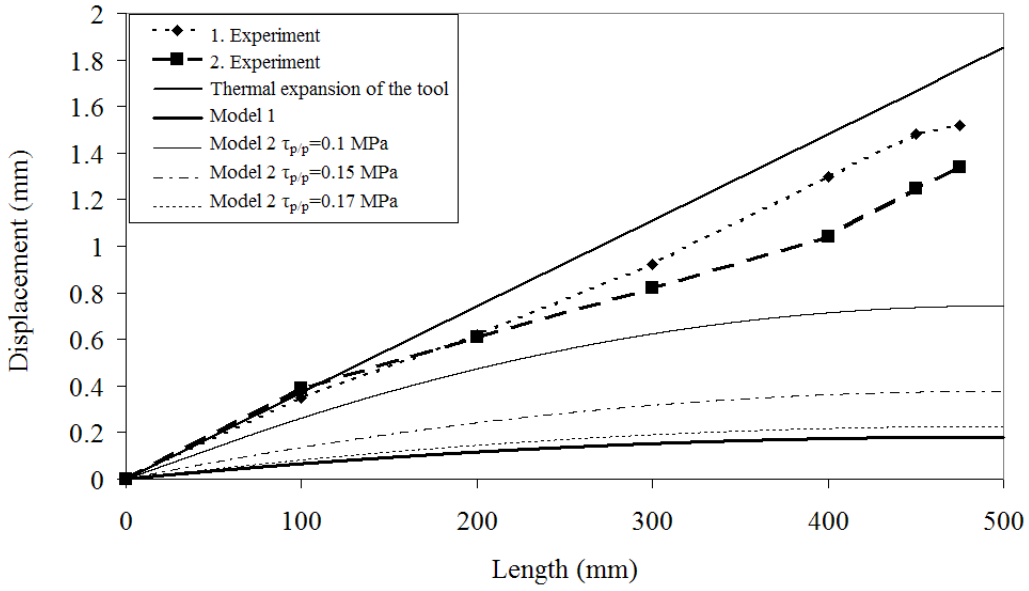

Figure 6.2. Displacement of $[0_8]$ specimen

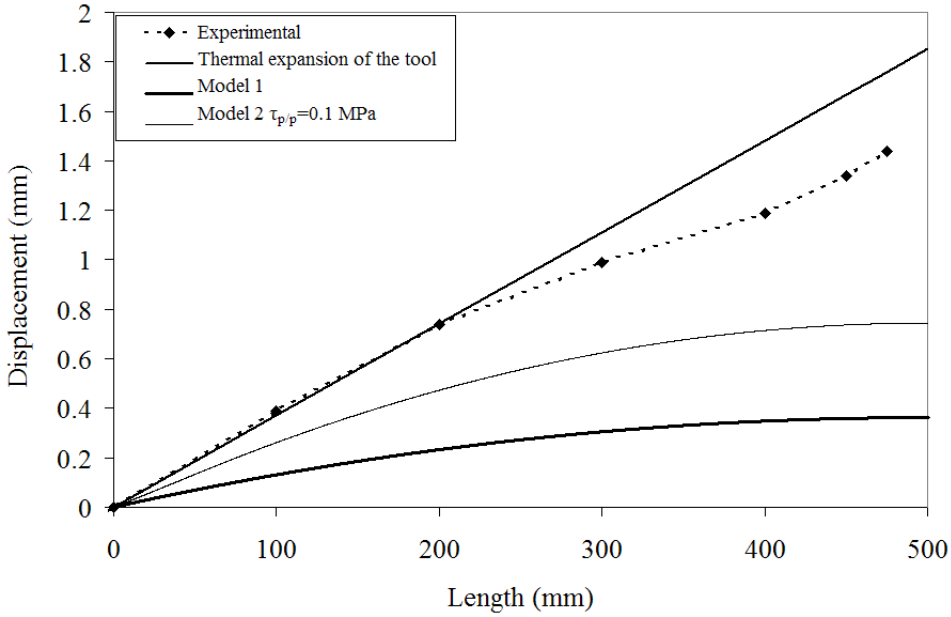

Figure 6.3. Displacement of $[0_2/90]_s$ specimen

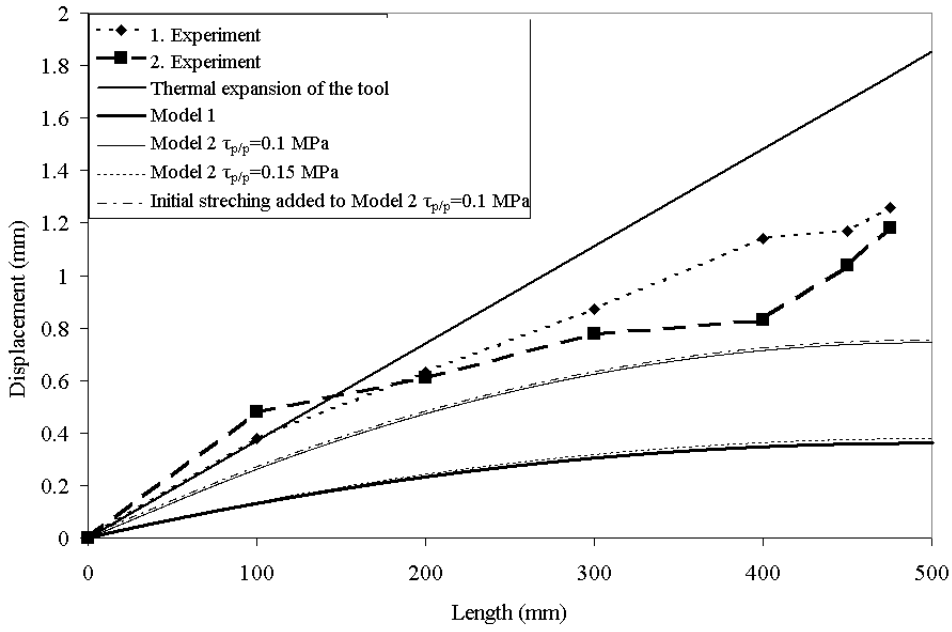

Figure 6.4. Displacement of $[0_2/90_2]_s$ specimen

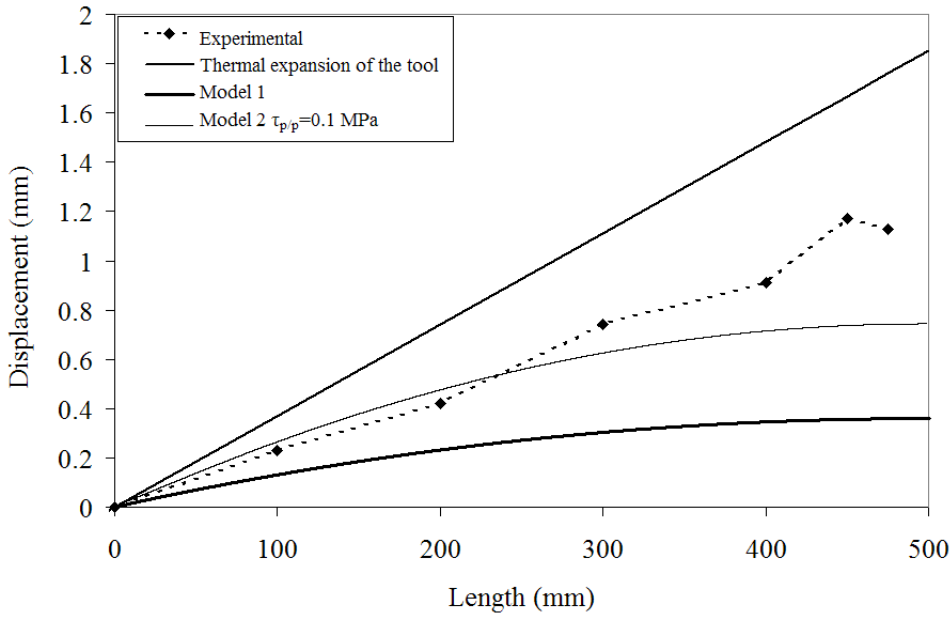

Figure 6.5. Displacement of $[0_2/90_3]_s$ specimen

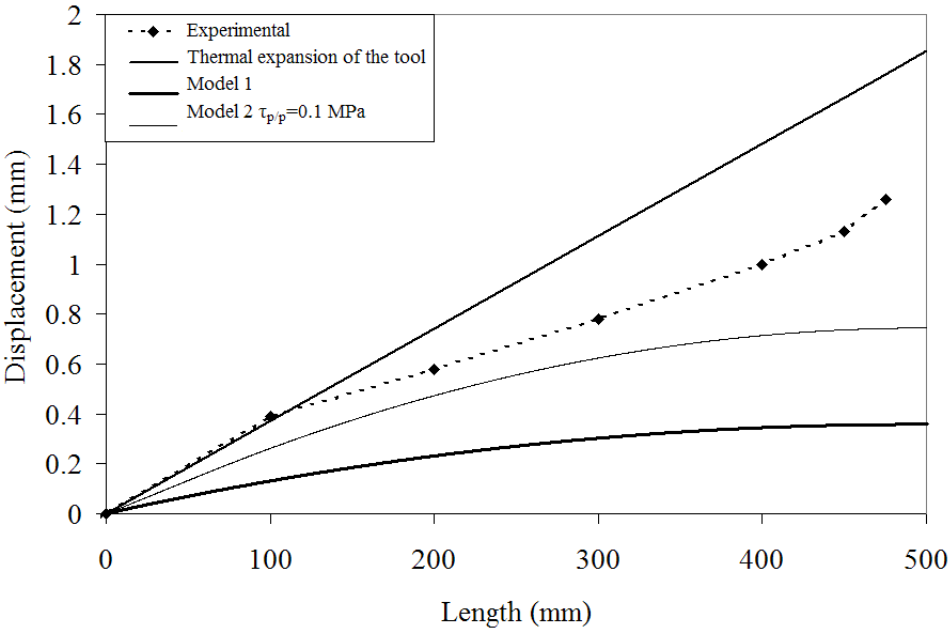

Figure 6.6. Displacement of $[0_2/90_4]_s$ specimen

6.3. Image Analysis

Sample pieces were cut from the corners of the 1m. long flat parts of $[0_8]$ $[0_2/90_2]_s$ and $[0_2/90_4]_s$ configurations and images were taken under the optic microscope. In these images, it can be seen that there is a slip and intraply shear of the bottom ply, which is in contact with the tool with respect to the other plies. The amount of slip is smallest in unidirectional composite part.

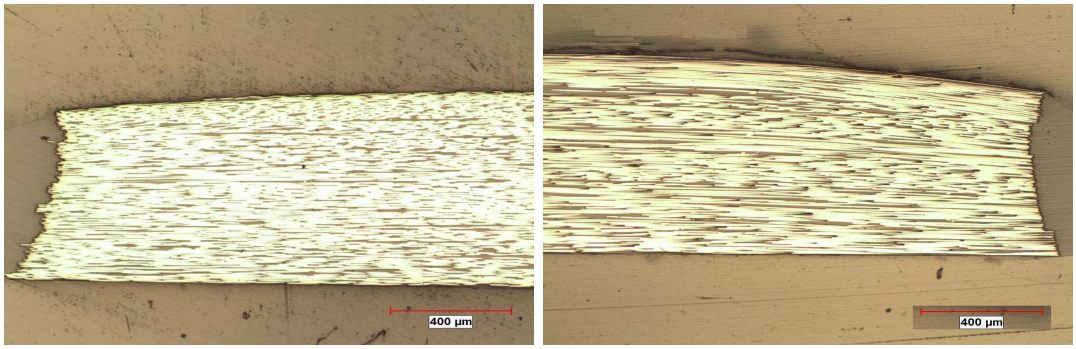

Figure 6.7. Microscope image from $[0_8]$ specimen

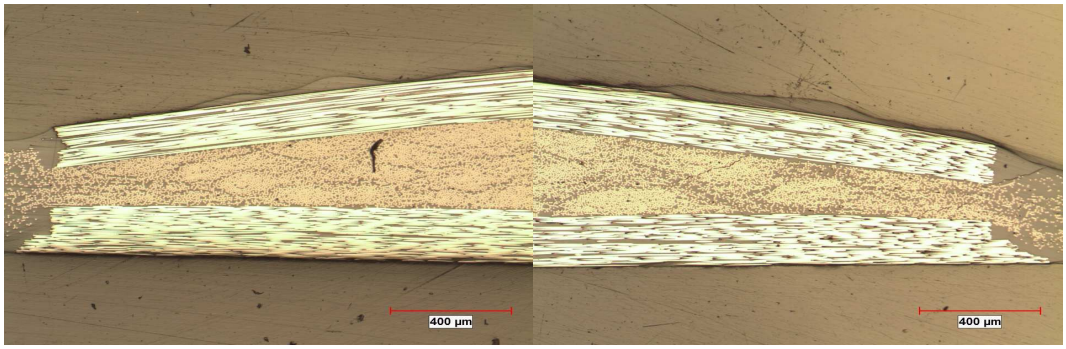

Figure 6.8. Microscope image from $[0_2/90_2]_s$

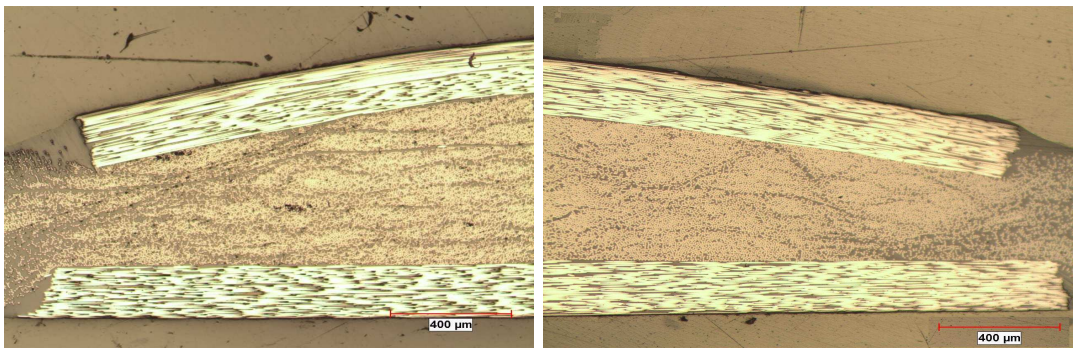

Figure 6.9. Microscope image from $[0_2/90_4]_s$

The relative displacement is measured directly from the microscope images. In Model 2, the node displacement at the end of the ply adjacent to the tool and the node displacement at the end of the ply at the bag side is measured. Then the difference is found to get the relative slipping. Then the amount of slip of the ply which is in contact with the tool measured from the images were compared with the analytical results. Comparison for all parts are listed in the Table 6.1 given below. Through this analysis, it is seen that the model predicts this slip at the end of the ply with a reasonable error margin when the maximum interply shear stress, $\tau_{p/p}$, is equal to 0.1 MPa. However for a higher interply shear stress $\tau_{p/p}$=0.15 MPa the difference of the relative slip between the nodel predictions and experimental observations are beyond a reasonable error margin.

Table 6.1. Image analysis compared to model results (R: Right End L: Left End)

	image results	Model 2 $\tau_{p/p}$=0.1	%difference	Model 2 $\tau_{p/p}$=0.15	%difference
$[0_8]$R	0.011764706	0.243541	15.01%	0.0848058	59.95%
$[0_8]$L	0.211764706				
$[0_2/90_2]_s$R	0.094117647	0.0570096	39.43%	0.001215	99.06%
$[0_2/90_2]_s$L	0.129411765				
$[0_2/90_4]_s$R	0.2	0.1947532	2.62%	0.001893	99.05%
$[0_2/90_4]_s$L	0.247058824				

6.4. Warpage

The method used for measuring the geometry of the 1 m long specimens, tproposed in the PhD thesis of Garstka [25], was to stand the strips on the edge on a sheet of paper and use a paint spray to transfer the edge geometry to the paper with minimal force. The distance between the straight line marked previously using a 1 m ruler and the sprayed line was measured using a digital caliper.

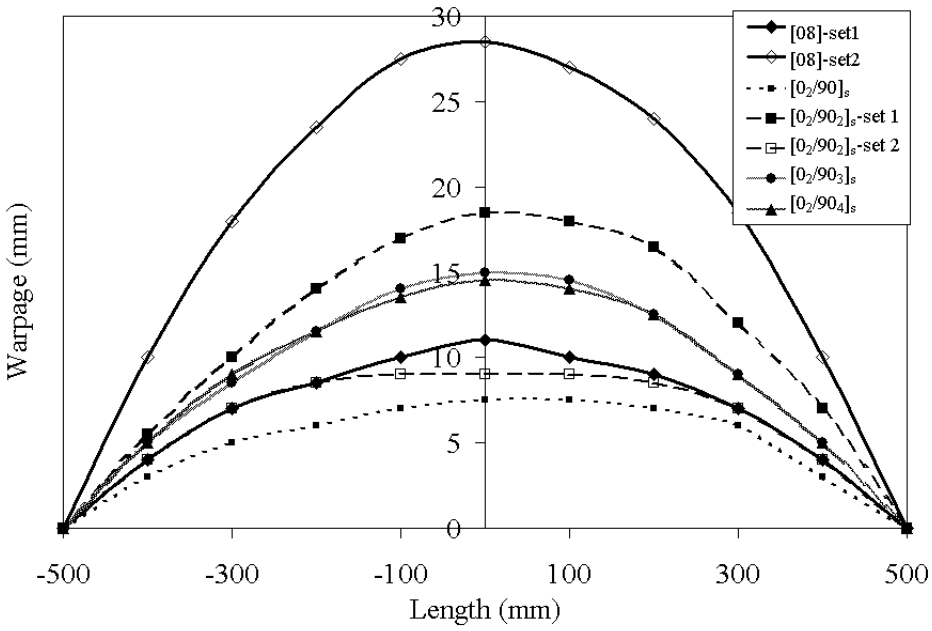

Figure 6.10. Experimental results for the warpage of 1 mm long part with different lay-ups.

In experiments, a distinguishable trend with respect to the lay-up was not observed. The results are plotted in Fig. 6.10. There are large differences in the warpage between two specimens of the identical lay-up. This variability can results from several reasons. Firstly, the prepregs were cut from a big roll. Since the prepregs were taken from different layers of this roll, the fibers may have different preloads on them. As getting closer to the inner radius, the fibers are more curved since they are rolled on a smaller diameter. Secondly, while laying up by hand, the fibers may be preloaded accidentally. Moreover, a surface imperfection or insufficient coating of release agent on the tool surface may induce unexpected frictional effects.

In Figs. 6.11 and 6.12, the results obtained from Model 1 and 2 are compared with the experimental results for $[0_8]$ and $[0_2/90_2]_s$ lay-ups. The interply shear stress $\tau_{p/p}$ is only an assumed value, so in order to find an upper bound and lower bound for this value, several trials were done.

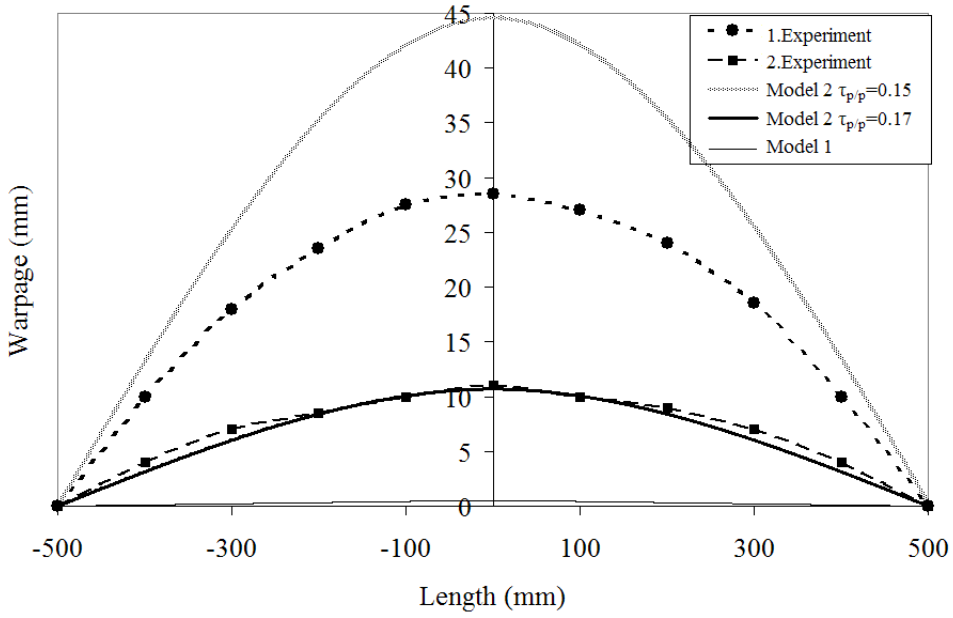

Figure 6.11. Comparison of experimental to analytical warpage results for $[0_8]$at the end of Step-3

In Figs. 6.11 and 6.12, it is seen that the results of Model 1 are below the experimental results for both lay-ups. Model 2 predicts warpage values much more closer to the experimental results when the interply shear stress $\tau_{p/p}$, is taken higher than 0.1 MPa. When $\tau_{p/p}$ is equal to 0.17 MPa in $[0_8]$ lay-up, the prediction is very close to the second experimental result. However this value of interply shear stress gives a very low interply slip as compared to the values measured by microscopic examinations.

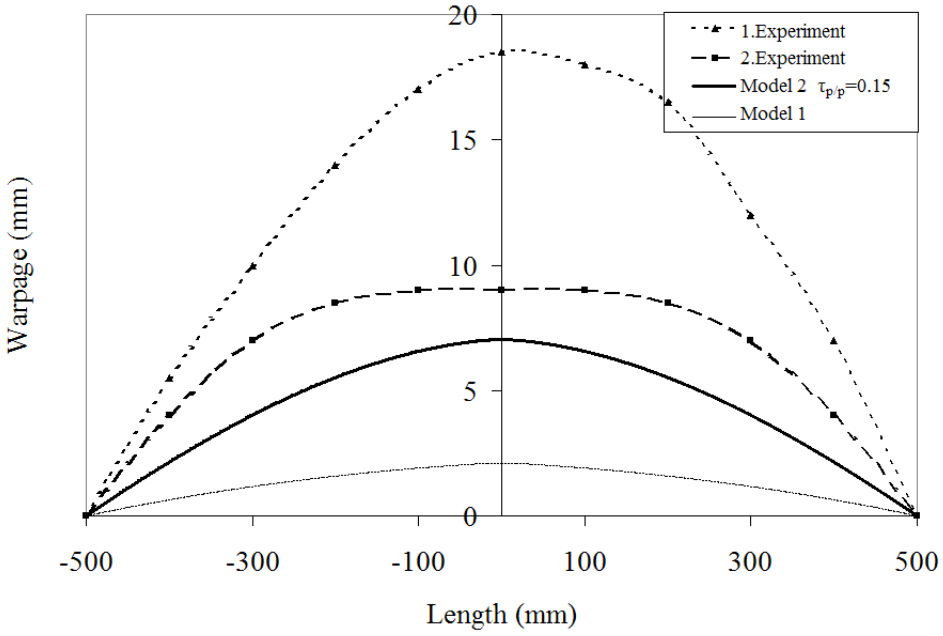

Figure 6.12. Comparison of experimental to analytical warpage results for $[0_2/90_2]_s$ at the end of Step-3

7. CONCLUSIONS

In this study, tool-part interaction induced warpage effects are modeled for flat composite strips in three different ways by using a two step finite element analysis procedure. The analysis is based on a number of simplifying assumptions, most of which are reasonable. Vitrification is treated as a point at which the material suddenly changes from the rubbery to glassy state with constant properties in each case.

As going far from the symmetry line of the part, the displacement increases linearly for all models. When we compare the results for Model 1 a and b, i.e. with and without tool, the results are pretty the same, which reveals that the modified model is good enough to reflect the effects of the tool. There is a parabolic trend only at regions close to the symmetry line. The reason for the deformation to be parabolic towards the symmetry line is the linear distribution of σ_{xx} (see Fig. 5.6) towards this line, elsewhere it is constant, hence causing no bending moment. In Model 2, the increasing parabolic behavior towards the symmetry line is better represented than the Model 1. However, the warpage depends greatly on the magnitude of the maximum interply shear stress. As $\tau_{p/p}$ increases, there is a less increase in σ_{xx} at interply contact, which means the moment resultant, hence the curvature due to this stress distribution is less.

For rubbery and glassy state of the part, 18 material properties are defined in the model. From these properties modulus in transverse direction E_{22}, shear moduli G_{12} and G_{23} have the most dominant role in modeling the deformation behavior of the composite part, because they can effect the residual stresses generated during the cure cycle. It is shown previously that the warpage depends greatly on the magnitude of the maximum interply shear stress. To have a more correct model representation, these parameters should be measured.

Through tension test, by loading and unloading a single ply, a load displacement data obtained, which is then converted into stress-strain relation. The difference be-

tween the loading and unloading curves reveals that the initial waviness of fibers are straightened with minimal force, causing an initial displacement without much fibre stress developing.

Marked-tool test showed that Model 2 is better than Model 1 to represent the displacement of the composite flat part along its length. But the interface shear stress seems to be higher than the value of 0.2 MPa.

Image analysis of the sample pieces cut from the corners of the 1 m long flat parts were used to compare the results obtained in the analytical work. In these images, it can be seen that there is a slip of the bottom ply which is in contact with the tool. The amount of slip is smallest in unidirectional composite part.

Warpage results obtained from experiments are less than the predictions of the models when the maximum interply shear stress, $\tau_{p/p}$, is equal to 0.1 MPa. The results get closer to the experimental data when $\tau_{p/p}$ is taken as 0.15 MPa. Moreover there are large differences in warpage values for two specimens of the same lay-up. The effects that can cause this are discussed in detail. Firstly, the prepregs were cut from a big roll. The prepregs were taken from different layers of this roll the fibers may have different preloads on them. As getting closer to the inner radius, the fibers are more curved since they are rolled on a smaller diameter.

REFERENCES

1. Ruiz, E. and F. Trochu, Numerical analysis of cure temperature and internal stresses in thin and thick RTM parts, *Composites: Part A* 36 (2005) 806-826.

2. Pagliuso, S., "Warpage A Nightmare for composite parts producers", *Progress in science and engineering of composites*, ICCM 4, pp. 1617-23,1982

3. Radford, W. D., "Cure Shrinkage Induced Warpage in Flat Uni-Axial Composite", *Journal of Composite Technology and Research, Vol. 15, No. 4*, pp.290-296, 1993

4. Cann, M. T. and D. O. Adams, "Effect of Part-Tool Interaction on the Cure Distortion of Flat Composite Laminates", *46th International SAMPE Symposium*, May 6-10 2001.

5. Radford D.W. and T.S. Rennick, "Separating Sources of Manufacturing Distortion in Laminated Composites", *Journal of Reinforced Plastics and Composites*, pp. 621-641,2000

6. Darrow, D. A. Jr. and L. V. Smith, "Isolating Components of Processing Induced Warpage in Laminated Composites", *Journal of Composite Materials, Vol. 36, No. 21*, 2002

7. Albert, C. and G. Fernlund, "Spring-in and warpage of angled composite laminates", *Composites Science and Technology*, pp. 1895-1912, 2002

8. Ferlund, G., N. Rahman, R. Courdji, M. Bresslauer, A. Poursartip, K. Willden, K. Nelson, "Experimental and numerical study of the effect of cure cycle, tool surface, geometry, and lay-up on the dimensional fidelity of autoclave-processed composite parts", *Composites: Part A*,pp. 33:341-351, 2002

9. Zhu, Q., P. H. Geubelle, M. Li, C. L. III Tucker, "Dimensional Accuracy of Ther-

moset Composites: Simulation of Process-Induced Residual Stresses", *Journal of Composite Materials*, pp. 35(24): 2171-2205, 2001

10. Johnston, A., *An integrated model of the development of process-induced deformation in autoclave processing of composites structures*, Ph.D. thesis, The University of British Columbia, Vancouver, 1997

11. Johnston, A., R. Vaziri and A. Poursartip, "A plane strain model for process-induced deformation of laminated composite structures", *Journal of Composite Materials*, pp. 1435-1469, 2001

12. Twigg, G., A. Poursartip and G. Fernlund, "An experimental method for quantifying tool-part shear interaction during composites processing", *Composites Science and Technology 63* , pp. 1985-2002, 2003

13. Twigg, G., A. Poursartip and G. Fernlund, "Tool-part interaction in composites processing. Part I: experimental investigation and analytical model", *Composites: Part A*, 35 pp. 121-133, 2004

14. Twigg, G., A. Poursartip and G. Fernlund, "Tool-Part Interaction in Composites Processing. Part II: Numerical Modelling", *Composites Part A*, 34 (11),2003

15. Kim, Y.K. and I.M. Daniel, "Cure Cycle Effect on Composite Structures Manufactured by Resin Transfer Molding", *Journal of Composite Materials*, Vol. 36, No. 14, 2002

16. Potter, K., M. Campbell and M. R. Wisnom, "Investigation of tool/part interaction effects in the manufacture of composite components", *Proceedings of ICCM-14, 14th International Conference on Composite Materials*, San Diego, USA, 14-18 June 2003

17. Flanagan R., "The dimensional stability of composite laminates and structures", PhD Thesis, Queen's University of Belfast, 1997.

18. Ersoy N.,Potter K., Wisnom M.R.,Clegg M. J., "An experimental method to study

the frictional process during composites manufacturing", *Composites: Part A* , pp. 1536-1544,2005

19. Wisnom M.R., M. Gigliotti, N. Ersoy, M. Campbell, K.D. Potter, "Mechanisms generating residual stresses and distortion during manufacture of polymer-matrix composite structures", *Composites: Part A* , pp. 522-529, 2006

20. Arafath, A. R. A., *Efficient numerical techniques for predicting process-induced stresses and deformations in composite structures*, PhD thesis, The University of British Columbia, Canada, 2007

21. Ersoy, N., Potter, K., Wisnom, M.R., "Modelling of the spring-in phenomenon in curved parts made of a thermosetting composite",to be published.

22. Wisnom, M.R., Ersoy, N., Potter, K.D., "Shear-Lag Analysis of the Effect of Thickness on Spring-in of Curved Composites", *Journal of Composites Materials*, in press.

23. Ersoy, N., T. Garstka, K. Potter, M. R. Wisnom, M. Clegg, "Development of the properties of a thermosetting resin and its carbon fibre composite through cure", to be published.

24. Hibbit, Karlsson and Sorensen Inc. ABAQUS Online Documentation, Version 6.5-1; 2004.

25. Garstka, T., *Separation of process induced distortions in curved composite laminates*, PhD thesis, The University of Bristol, 2005